Agricultural and Forest Meteorology 256–257 (2018) 253–269

Contents lists available at ScienceDirect

Agricultural and Forest Meteorology

journal homepage: www.elsevier.com/locate/agrformet

BESS-Rice: A remote sensing derived and biophysical process-based rice productivity simulation model

Yan Huang[a], Youngryel Ryu[a,b,c,d,*], Chongya Jiang[d], Hyungsuk Kimm[b], Soyoun Kim[b], Minseok Kang[e], Kyomoon Shim[f]

[a] Research Institute of Agriculture and Life Sciences, Seoul National University, South Korea
[b] Department of Landscape Architecture and Rural Systems Engineering, Seoul National University, South Korea
[c] Interdisciplinary Program in Agricultural and Forest Meteorology, and in Landscape Architecture, Seoul National University, South Korea
[d] Brain Korea 21 Plus Team, Seoul National University, South Korea
[e] National Center for Agro Meteorology, South Korea
[f] National Institute of Agricultural Sciences, Rural Development Administration, South Korea

ARTICLE INFO

Keywords:
Crop modeling
Carbon allocation
Gross primary productivity
Yield
Rice
BESS

ABSTRACT

Conventional process-based crop simulation models and agro-land surface models require numerous forcing variables and input parameters. The regional application of these crop simulation models is complicated by factors concerning input data requirements and parameter uncertainty. In addition, the empirical remotely sensed regional scale crop yield estimation method does not enable growth process modeling. In this study, we developed a process-based rice yield estimation model by integrating an assimilate allocation module into the satellite remote sensing-derived and biophysical process-based Breathing Earth System Simulator (BESS). Normalized accumulated gross primary productivity ($GPP_{norm-accu}$) was used as a scaler for growth development, and the relationships between $GPP_{norm-accu}$ and dry matter partitioning coefficients were determined from the eddy covariance and biometric measurements at the Cheorwon Rice paddy KoFlux site. Over 95% of the variation in the dry matter allocation coefficients of rice grain could be explained by $GPP_{norm-accu}$. The dynamics of dry matter distribution among different rice components were simulated, and the annual grain yields were estimated. BESS-Rice simulated GPP and dry matter partitioning dynamics, and rice yields were evaluated against *in-situ* measurements at three paddy rice sites registered in KoFlux. The results showed that BESS-Rice performed well in terms of rice productivity estimation, with average root mean square error (RMSE) value of 2.2 g C m^{-2} d^{-1} (29.5%) and bias of –0.5 g C m^{-2} d^{-1} (–7.1%) for daily GPP, and an average RMSE value of 534.8 kg ha^{-1} (7.7%) and bias of 242.1 kg ha^{-1} (3.5%) for the annual yield, respectively. BESS-Rice is much simpler than conventional crop models and this helps to reduce the uncertainty related to the forcing variables and input parameters and can result in improved regional yield estimation. The process-based mechanism of BESS-Rice also enables an agronomic diagnosis to be made and the potential impacts of climate change on rice productivity to be investigated.

1. Introduction

The challenges of food security and regional food inequalities will update over time due to the rapid increase in global food demand and aggravation of climate change (Tilman et al., 2011; Wheeler and Von Braun, 2013). Hence, there is an urgent need to accelerate food production and productivity. The sustainable intensification of crop production is therefore of great importance (Reddy, 2016). Successful crop productivity estimations are important for cultivation management and agricultural decision-making (Hochman et al., 2009; Kassie et al., 2016). The estimation of accurate crop production also facilitates a better understanding of the way crop growth and production responses to environmental factors (Bregaglio et al., 2017; Guan et al., 2016; Tollenaar et al., 2017).

Process-based crop simulation models use quantitative descriptions of ecophysiological processes to simulate crop growth and development as influenced by environmental conditions and management practices (Hodson and White, 2010). Therefore process-based crop simulation models can be used to understand the mutual effects among crop genotypes, management, and the environment (Messina et al., 2009). These

* Corresponding author at: College of Agriculture and Life Sciences, Seoul National University, 1 Gwanak-ro, 200-9217, Gwanak-gu, Seoul, South Korea.
E-mail address: yryu@snu.ac.kr (Y. Ryu).

https://doi.org/10.1016/j.agrformet.2018.03.014
Received 15 November 2017; Received in revised form 16 March 2018; Accepted 20 March 2018
Available online 30 March 2018
0168-1923/

crop simulation models have also been widely used to investigate the potential impacts of climate change on agricultural productivity (Asseng et al., 2015; Rosenzweig et al., 2014) and to explore the management options under current growing situations (Hochman et al., 2009; Kassie et al., 2016). Moreover, agro-land surface model, which is a land surface model or dynamic vegetation model incorporated with a crop simulation model, is a useful tool for simulating the fluxes of heat, water, and gases in agricultural land (Masutomi et al., 2016a).

Conventional process-based crop simulation models and agro-land surface models, however, require numerous forcing variables, including genetic specific data, soil physicochemical characteristics, management practices, and agro-meteorological data; and input parameters, including soil-type specific, crop specific, simulation setting, and other coefficients. (Li et al., 2015; Masutomi et al., 2016a). The regional application of such models is complicated and hampered by factors concerning input data requirements and parameter uncertainty. Information regarding regional differences in crop management, cultivar distributions, and coefficients for parameterizing agro-environmental processes are usually unavailable (Folberth et al., 2016a). Previous studies have shown that the uncertainties of crop cultivars and management (Folberth et al., 2016a), soil characteristics (Folberth et al., 2016b; Varella et al., 2012), meteorological conditions (Li et al., 2015; Zhao et al., 2015), and parameters settings (Ramirez-Villegas et al., 2017; Tao et al., 2018) all influence the accuracy of crop production simulation. Relatively, regional agro-meteorological variables are available from the reanalysis datasets, which are derived from the systematic approach based on surface observations, models and data assimilation (Rienecker et al., 2011).

Remote sensing can provide temporally and spatially continuous information regarding crop biophysical variables and estimates of crop yield (Battude et al., 2016; Burke and Lobell, 2017; Lobell et al., 2015). The usefulness of remote sensing for interpreting the process of crop production and how it responds to environmental factors, however, is clearly inferior compared with the process-based crop simulation models. Recent studies have revealed that crop yield can be reliably estimated from the satellite-based crop gross primary productivity (GPP) (Guan et al., 2016; Xin et al., 2013; Yuan et al., 2016). Such estimations are based on the use of a crop-specific harvest index (HI) to convert net primary productivity (NPP) data to yield at the harvest time, which does not consider the process of yield formation. Yuan et al. (2016) simulated different types of crop yield based on the satellite-based light use efficiency model derived GPP estimations at 12 sites across Europe and North America, using HI and a constant carbon allocation coefficient and did not take into account temporal or spatial variations. The results showed that yield was underestimated by between 61% and 32% at several sites and overestimated from 34% to 55% at other sites in their study.

Integrating remote sensing information and process-based crop simulation models can maximize their advantages. Remote sensing can support crop modeling by monitoring vegetation status at regional scale, which would be very difficult to obtain otherwise (Dorigo et al., 2007). Process-based crop simulation models can dynamically simulate the carbon, nitrogen, and water balances at daily or hourly time-steps to estimate crop growth and development (Boote et al., 2013). Many studies improved the crop growth simulation and yield estimation using the data-model integration approaches (Casa et al., 2012; Huang et al., 2013; Jin et al., 2017; Zhang et al., 2016). Almost all these previous studies have used remote sensing-derived vegetation indices or biophysical and biochemical variables, e.g., leaf area index (LAI), biomass or leaf nitrogen accumulation, to improve the crop simulation processes. However, the number of the remote sensing derived variables in these studies is very limited compared to the large number of forcing variables required by the crop simulation models. Many forcing variables of the crop simulation models were still unavailable regionally and a limited range of field measurements has therefore been used. Therefore, integrating as much remote sensing information as possible to a process-based crop simulation model and trying to simplify the requirement of forcing variables of this model are very important for regional crop growth simulation and productivity estimation.

The Breathing Earth System Simulator (BESS) model is a highly simplified remote sensing-derived and biophysical process model. BESS couples the processes of atmosphere (Ryu et al., 2018) and canopy radiative transfer, canopy photosynthesis, evapotranspiration, and energy balance, and has been proven to perform well in estimating GPP (Jiang and Ryu, 2016; Ryu et al., 2011). BESS uses an enzyme kinetic model (Farquhar et al., 1980) to estimate GPP, which offers a more mechanistic interpretation than empirical approaches, such as light use efficiency-based models. As a remote sensing forced process-based model, BESS could provide a comprehensive understanding and description of key ecological processes in agro-ecosystems on global scale and with a spatial resolution of 1 km. However, because it lacks an assimilate allocation module, BESS cannot be applied for crop growth simulation and yield estimation. After filling this gap, BESS could be used as a remote sensing derived process-based crop simulation model, and is expected to be simpler than conventional crop simulation models in terms of variable requirements.

Rice (*Oryza sativa L.*) is one of the three leading food crops worldwide and is consumed by over half of the world's population (Maclean et al., 2013). Under climate change, rice production has become vulnerable to extreme weather events and gradual climate risks (Ainsworth, 2008; Kim et al., 2013; Simelton et al., 2012). Therefore, it is important to accurately simulate growth and estimate the productivity of rice. The existing rice simulation models, e.g. APSIM-ORYZA (Gaydon et al., 2012a,b), CERES-Rice (Singh et al., 1993), and DNDC-Rice (Fumoto et al., 2010) all require dozens of genotype data, soil characteristics, cultivation practices, and meteorological information as forcing variables. Developing a variable-simplified and remote sensing-derived rice simulation model is important for regional rice growth simulation and productivity estimation, and would have further applications in agricultural decision making and climate change research.

The goals of this study were: 1) to develop a remote sensing-derived and process-based rice productivity simulation model, BESS-Rice, by integrating the assimilate allocation module into BESS; 2) to evaluate the accuracy of BESS-Rice by comparing the simulated GPP, dry matter partitioning, and grain yield against *in-situ* measurements at site-level; and 3) to analyze the sensitivity of BESS-Rice to environmental and biological drivers and parameters.

2. Material and methods

2.1. Overview of sites and data

Three KoFlux rice paddy sites (http://www.ncam.kr/page/koflux/database/), distributed from north to south in South Korea were used in this study (Fig. 1): Cheorwon (CRK; 38.2013°N, 127.2507°E), Cheongmicheon (CFK; 37.1597°N, 127.6536°E), and Gimje (GRK; 35.7451°N, 126.8524°E). Both CRK and CFK have a monsoon and temperate continental climate, with cold and dry winters, and hot summers; GRK has a temperate monsoon climate with marine climate characteristics, with a cold winter and hot summer, without a dry season (Peel et al., 2007). The 30-year mean annual precipitation at CRK, CFK and GRK are 1391 mm, 1371 mm and 1253 mm, and the mean annual air temperature are 10.2 °C, 11.6 °C and 12.9 °C, respectively (Korea Meteorological Administration). The elevation of these three sites are approximately 175 m, 60 m and 21 m above sea level based on the Advanced Spaceborne Thermal Emission and Reflection Radiometer (ASTER) Global Digital Elevation Model (GDEM), and the soil types are silty clay loam, sandy loam and silt loam based on the national soil database (Hong et al., 2009b) from Rural Development Administration of South Korea. Irrigated japonica rice (*Oryza sativa* L. ssp. *japonica*) varieties were cultivated at all three sites. These are the predominant rice subspecies

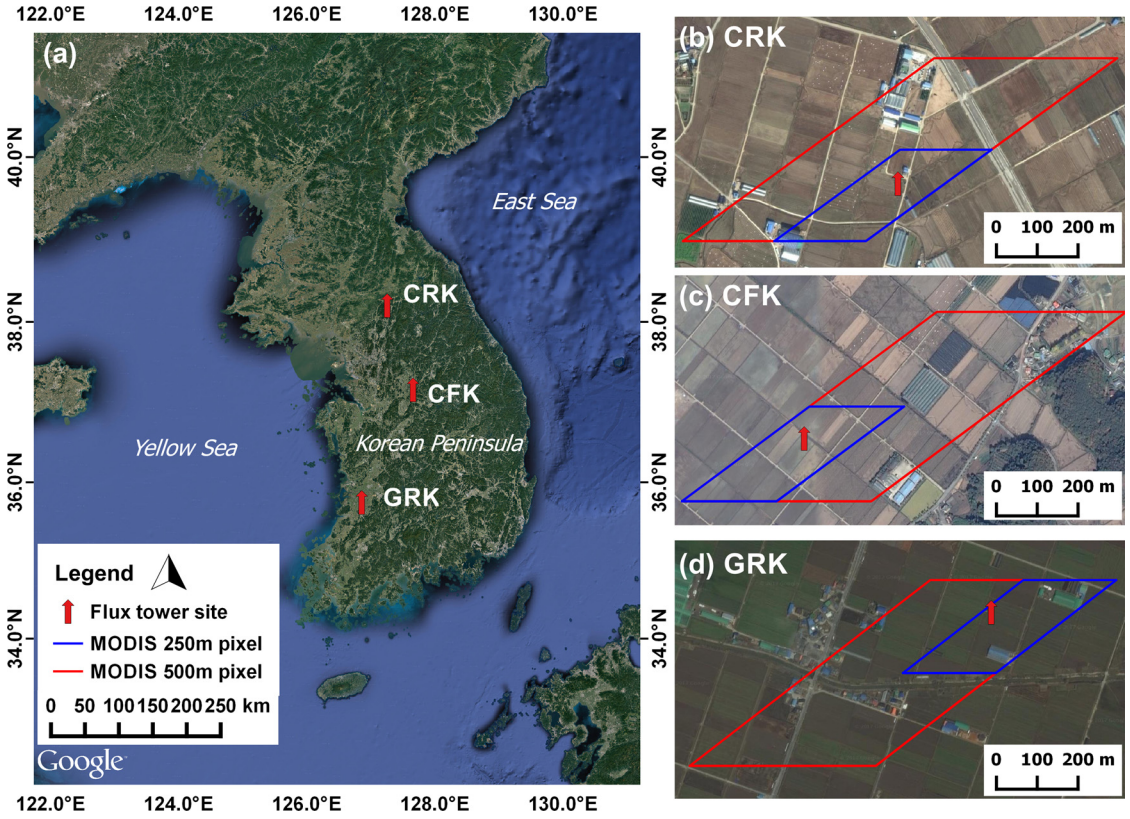

Fig. 1. Location of the study sites. (a) Locations of Cheorwon (CRK), Cheongmicheon (CFK) and Gimje (GRK) sites; (b) CRK site; (c) CFK site; (d) GRK site.

planted in the Korean Peninsula. Single cropping rice was cultivated at CRK and CFK in a year. Rice at CRK, in 2015, was transplanted in mid-May (day of year [DOY] 135) and harvested in mid-September (DOY 257); while in 2016, rice was transplanted in late-April (DOY 120) and harvested in early-September (DOY 245). At CFK, rice was also transplanted in mid-May and harvested in mid-late September. At GRK, barley and paddy rice rotation was conducted in a year, and rice was transplanted in mid-late June and harvested in mid-late October (Kim et al., 2016; Min et al., 2013; Xin et al., 2017). A brief description of these sites is given in Table 1.

Eddy covariance (EC)-derived GPP and dry mass proportional data (explained in Sections 2.2 and 2.4) from CRK in 2015 and 2016 was used to develop the carbon allocation module of the BESS-Rice model. Satellite data, mainly including Moderate Resolution Imaging Spectroradiometer (MODIS), and reanalysis datasets (Jiang and Ryu, 2016) for the three sites in different years were used as forcing data for BESS-Rice (explained in Sections 2.2 and 2.4). Field measurements including EC-derived GPP, the dry mass proportion, and yield were used for evaluating BESS-Rice simulations (explained in Sections 2.3 and 2.4).

2.2. Development of BESS-rice

The BESS-Rice model was constructed by integrating the newly developed assimilate allocation module into the existing BESS model. BESS-Rice has a daily time-step and was built into three main modules (Fig. 2) of dry matter accumulation, dry matter partitioning, and yield formation.

2.2.1. Dry matter accumulation

2.2.1.1. BESS model and GPP simulation. BESS couples a series of models of the processes of atmosphere and canopy radiative transfer, canopy photosynthesis, evapotranspiration, and energy balance. A one-dimensional atmospheric radiative transfer model from the Forest Light Environmental Simulator (FLiES) (Kobayashi and Iwabuchi, 2008) was used to calculate incoming shortwave radiation, photosynthetic active radiation (PAR), and near-infrared radiation (NIR) for both the beam and diffuse components at the top of the canopy (Ryu et al., 2018). A two-leaf and two-stream canopy radiative transfer model was used in BESS to quantify the absorbed PAR and NIR (De Pury and Farquhar, 1997; Goudriaan, 1977). A carbon-water coupled module, including a two-leaf longwave radiative transfer model (Wang and Leuning, 1998), Farquhar's photosynthesis model for C3 plants (Farquhar et al., 1980), a stomatal conductance equation (Ball, 1988), and the quadratic Penman-Monteith and energy balance equations (Paw U, 1987; Paw U and Gao, 1988), was used to compute GPP for sunlit and shaded canopies through the carbon-water interactive iterative procedure (Jiang and Ryu, 2016; Ryu et al., 2011).

The peak value of the maximum rice leaf carboxylation capacity at 25 °C ($V_{max}^{25°C}$) over the whole growing season was used to replace the $V_{max}^{25°C}$ value from the plant functional type (PFT) dependent look-up table. This peak $V_{max}^{25°C}$ (set as a constant with a value of 120 μmol m^{-2} s^{-1}) was determined at CRK in 2016 from leaf gas exchange measurements, with a portable photosynthesis system (Li-6400; LI-COR Inc., Lincoln, NE, USA) and calculated using the Microsoft Excel™ spreadsheet provided by Sharkey et al. (2007). The satellite data-derived instantaneous estimates of GPP were temporally up-scaled to daily estimates using a simple cosine function (Ryu et al., 2012). Finally, BESS-Rice was developed at a daily time-step based on the daily GPP estimates.

The forcing data for BESS-Rice were daily atmospheric temperature (T_a), daily dew point temperature (T_d), wind speed (WS), PAR, LAI, albedo, clumping index (CI) and the NDVI derived from MODIS atmosphere and land products and downscaled Modern-Era Retrospective Analysis for Research and Applications (MERRA) reanalysis data (Jiang and Ryu, 2016). More information regarding the preparation of forcing data was given in Section 2.4.1.

2.2.1.2. Dry mass simulation. Daily accumulated NPP ($\sum_{i=1}^{n} NPP$,

Table 1
Site information.

Site ID	Latitude	Longitude	Elevation (m)	Mean annual precipitation (mm)	Mean annual air temperature (°C)	Soil type	Year	Transplanting (DOY)	Booting (DOY)	Harvest (DOY)	Peak LAI	Stem density (hills m^{-2})	NPP (g C m^{-2})	Grain moisture (%)	Yield (kg ha^{-1})
CRK	38.20 °N	127.25 °E	175[a]	1391.2[b]	10.2[b]	Silty clay loam[c]	2015	135	193	257	5.54	23.6	–	–	8127.9
							2016	120	181	245	5.27	17.0	663.44	8.35	8231.8
CFK	37.16 °N	127.65 °E	60[a]	1370.8[b]	11.6[b]	Sandy loam[c]	2016	136	200	264	5.32	19.5	479.78	10.11	6011.0
GRK	35.75 °N	126.85 °E	21[a]	1253[d]	12.9[d]	Silt loam[c]	2011	170[e]	220[e]	289[e]	5.59	27.8	–	14	6591.6
							2012	173[e]	225[e]	294[e]	5.17	22.2	489.00[f]	14	5714.8
							2014	160[e]	216[e]	285[e]	5.19	22.2	–	14	7067.9

DOY: day of year; LAI, leaf area index; NPP, net primary productivity; CRK, Cheorwon site; CFK, Cheongmicheon site; GRK, Gimje site.

[a] ASTER GDEM, http://www.jspacesystems.or.jp/ersdac/GDEM/E/index.html.

[b] Korea Meteorological Administration, http://www.kma.go.kr/index.jsp.

[c] Hong et al., 2009a,b.

[d] Xin et al., 2017.

[e] Kim et al., 2016.

[f] Min et al., 2013.

$g\,C\,m^{-2}$) values were calculated from BESS simulated GPP ($g\,C\,m^{-2}\,d^{-1}$) using the NPP/GPP ratio (φ) over the whole rice growing season (n is the number of days of the growing season):

$$\sum_{i=1}^{n} NPP = \varphi \sum_{i=1}^{n} GPP \tag{1}$$

Daily dry mass of total rice plant (W_t, $g\,m^{-2}$) values were calculated based on the carbon content (ρ_c, unitless) of the rice plant. The carbon content is relatively consistent among different components of rice plants over the whole growing season according to the 2015 field measurements at CRK, with the seasonally averaged values of 0.42 (± 0.004) for leaves, 0.40 (± 0.003) for stems, 0.42 (± 0.002) for grains, and 0.40 (± 0.011) for roots. We present data as the mean (± 95% confidence interval) here. A constant value of carbon content for the whole plant was set as 0.4 in this study.

$$W_t = \sum_{i=1}^{n} NPP/\rho_c \tag{2}$$

2.2.2. Phasic development and dry matter partitioning

Daily normalized accumulated GPP ($GPP_{norm-accu}$) was used as a scaler to quantify the rice phenological development rate. This is defined as the ratio of daily accumulated GPP and the maximum accumulated GPP over the whole growing season (i.e., at harvest time) ($GPP_{max-accu}$).

$$GPP_{norm-accu} = GPP_{accu}/GPP_{max-accu} \tag{3}$$

The beginning of booting stage could be determined by $GPP_{norm-accu}$ with the threshold of 0.37 based on the averaged value (± 0.01) of EC-derived $GPP_{norm-accu}$ at the observed start of booting stage at CRK. Two stages of the growing season could then be detected. When $GPP_{norm-accu}$ is less than 0.37, it is the vegetative period and the dry mass of grain is 0; when $GPP_{norm-accu}$ is greater than 0.37, it is the reproductive phase and the dry mass of grain is increasing.

Relationships between $GPP_{norm-accu}$ and dry matter partitioning coefficients were developed for each component over the whole growing season using the EC-derived GPP and dry mass data at CRK in 2015 and 2016. The dry matter partitioning coefficients (ρ, unitless) for leaves (l), stems (s), grains (g) and belowground parts (b) (i.e. roots) were defined as the proportion of leaves, stems and grains against the aboveground (a) dry mass and the proportion of belowground dry mass against the total (t) plant dry mass, respectively. Gaussian and quadratic exponential relationships were fitted for the aboveground and belowground component dry matter partitioning coefficients with $GPP_{norm-accu}$, respectively, using the *in-situ* measurements at CRK in 2015 and 2016 (Fig. 3).

$$\rho_b = 0.35e^{-2.13GPP_{norm-accu}} + 0.003e^{3.23GPP_{norm-accu}} \tag{4}$$

$$\rho_l = 0.46e^{-\left(\frac{GPP_{norm-accu}-0.02}{0.74}\right)^2} \tag{5}$$

$$\rho_s = 0.64e^{-\left(\frac{GPP_{norm-accu}-0.35}{0.74}\right)^2} \tag{6}$$

$$\rho_g = 0.57e^{-\left(\frac{GPP_{norm-accu}-0.98}{0.35}\right)^2} \tag{7}$$

Dry matter weights () for different components were then calculated according to the dry matter partitioning coefficients.

$$W_t = W_a + W_b \tag{8}$$

$$W_b = W_t \times \rho_b \tag{9}$$

$$W_x = W_a \times \rho_x,\ x = l,\ s,\ g; \tag{10}$$

2.2.3. Yield formation

Finally rice yield could be calculated by the grain dry mass in the harvest ($W_{g-harvest}$) and the grain moisture content (C_m) at that time.

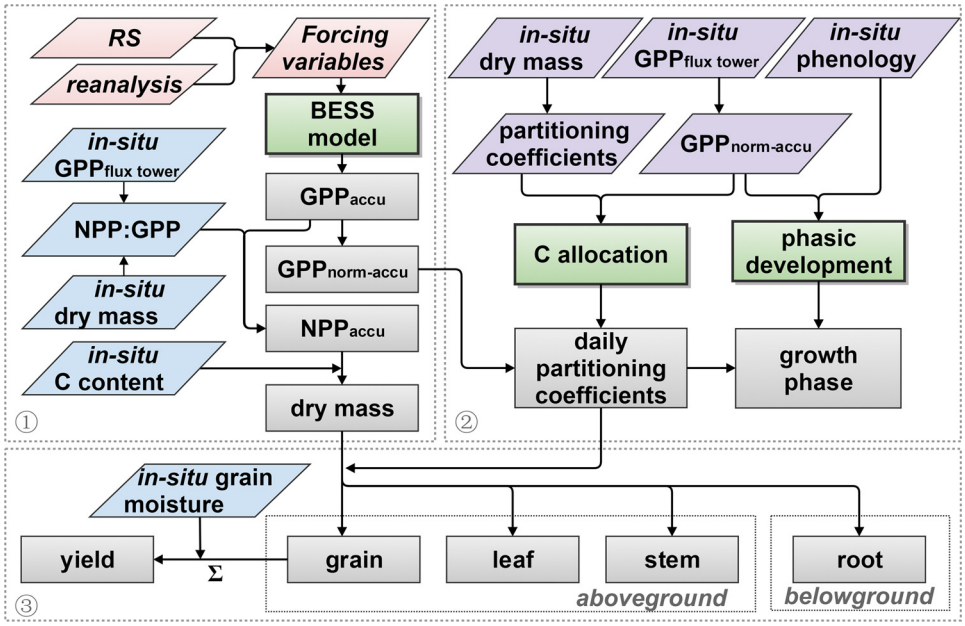

Fig. 2. Structure and data flow of the Breathing Earth System Simulator (BESS)-Rice model (① dry matter accumulation; ② dry matter partitioning and phasic development; and ③ yield formation). Parallelograms mean raw data or the variables and parameters derived from in-situ measurements or other datasets; red background indicates forcing variables; blue indicates input parameters; and purple indicates data used for model developing. Gray rectangles mean variables calculated in BESS-Rice model and green rectangle means model or modules. Σ indicates the grain dry mass accumulated. RS: remote sensing; C: carbon; NPP: net primary productivity; GPP: gross primary productivity; $GPP_{norm-accu}$: normalized accumulated GPP. (For interpretation of the references to colour in this figure legend, the reader is referred to the web version of this article).

$$Yield = W_{g-harvest}/(1-C_m) \quad (11)$$

2.3. Evaluation and sensitivity analysis of BESS-rice

For BESS-Rice evaluation in this study, the satellite and reanalysis data derived T_a, T_d, WS, PAR, LAI, albedo, CI and NDVI were all

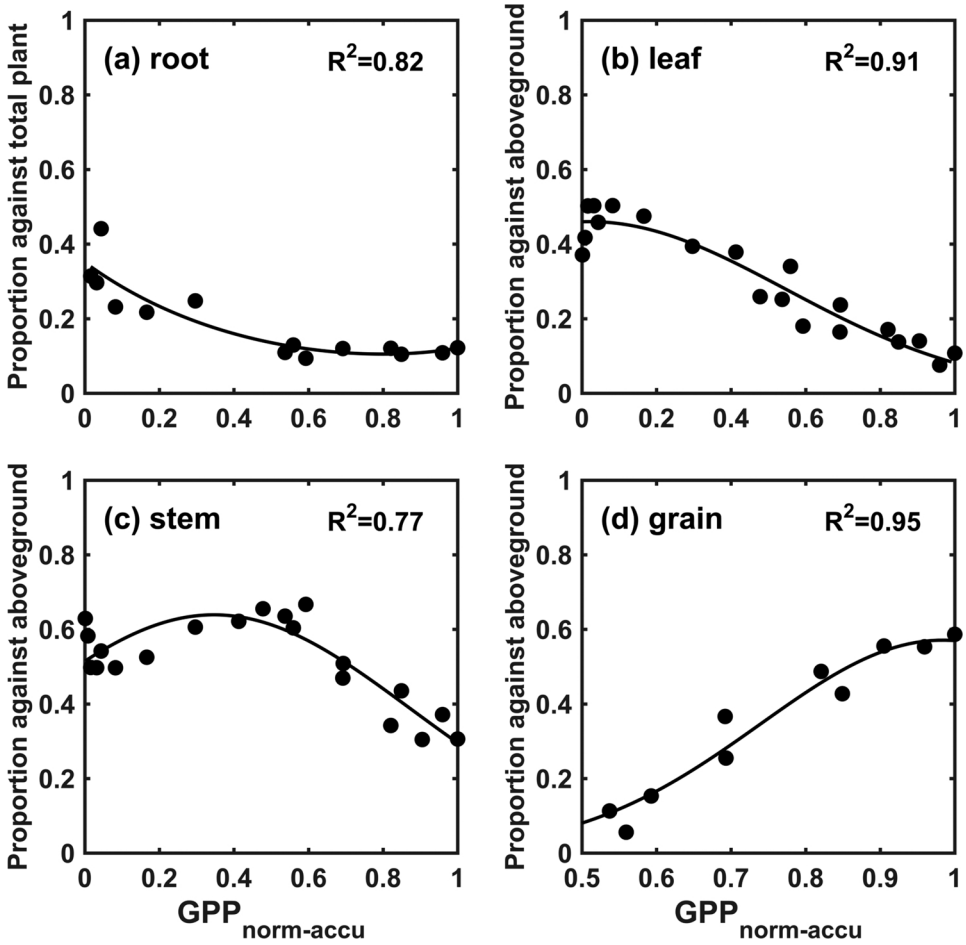

Fig. 3. Relationships between $GPP_{norm-accu}$ and dry matter partitioning coefficients (a, root; b, leaf; c, stem; and d, grain). Data is from flux tower-based eddy covariance (EC) GPP and *in-situ* measured dry mass at CRK in 2015 and 2016.

interpolated into daily intervals and used as model forcing data. The simulated GPP and $GPP_{norm-accu}$ at the daily scale and the annual grain yield were evaluated against the EC-based daily GPP and $GPP_{norm-accu}$ estimates and field measured yield, respectively, at all available sites. The simulated start of booting stage was compared with the field observed booting stage dates at CFK and GRK. The simulated dry mass proportion values of different rice components were compared with *in-situ* measurements only at the CRK site due to the unavailability of this data at the other sites. The root mean square error (RMSE), relative RMSE, bias, relative bias and coefficient of determination (R^2) were used to quantify the fitness between the simulated and measured values. A brief description of model forcing variables and evaluation data is given in Table A1 in Appendix A, and more information regarding the data preparation and measurement was given in Section 2.4.

The sensitivity of the BESS-Rice simulated GPP and yield to both environmental and biological forcing variables and input parameters were analyzed using a global sensitivity analysis (SA) method (Marino et al., 2008; Vanuytrecht et al., 2014; Xiao et al., 2014). It evaluates the relative importance of each forcing variable and input parameter in BESS-Rice, and can be used to identify the most influential variables affecting the model simulations (Saltelli et al., 1999; Verrelst et al., 2015). One of the most popular global SA method, the extended Fourier amplitude sensitivity test (eFAST) (Marino et al., 2008; Saltelli et al., 2008,1999) was applied in this study. Key parameters in this SA algorithm, the number of search curves and the number of samples per search curve were set as 100 and 1000, respectively. The total-order sensitivity index (S_T) was used to quantify the variable and parameter sensitivity over the whole rice growing season, which represents both the contribution of each forcing variable and input parameter to the variability of the model output and the interactions with other variables and parameters. To calculate S_{Ti} of a given parameter i (Marino et al., 2008; Saltelli et al., 2008), the first-order sensitivity index S_i was calculated as the variance (s_i^2) at a particular parameter's unique frequency divided by total variance.

$$S_i = s_i^2 / s_{total}^2 \tag{12}$$

s_i^2 was calculated from the Fourier coefficients at the frequency of interest, j :

$$s_i^2 = 2(A_j^2 + B_j^2) \tag{13}$$

where

$$A_j = \frac{1}{\pi}\int_{-\pi}^{\pi} f(x)\cos(jx)dx \tag{14}$$

$$B_j = \frac{1}{\pi}\int_{-\pi}^{\pi} f(x)\sin(jx)dx \tag{15}$$

S_{Ti} was calculated as the remaining variance after the contribution of the complementary set (i.e. all parameters except i). S_{Ci} is the summed S_i of the entire complementary set.

$$S_{Ti} = 1 - S_{Ci} \tag{16}$$

The forcing variables and the input parameters of BESS-Rice were analyzed. The forcing variables include T_a, T_d, WS, PAR, fraction of diffuse PAR (f_{dif}), LAI, white sky albedo in the visible range ($ALB_{WSA-VIS}$), white sky albedo in the near-infrared range ($ALB_{WSA-NIR}$), CI and peak $V_{max}^{25°C}$. The input parameters include φ, ρ_c, and C_m. The variation ranges of the forcing variables and input parameters were set based on the multi-year datasets of these variables and parameters and the reasonable range, which are listed in Table 2.

2.4. Measurement instruments and preprocessing

We provided details of all the satellite data, *in-situ* tower-based and other field measurements, used in this research in Table A1 in Appendix A. All the data processing was conducted using MATLAB® (The MathWorks, Inc., Natick, MA, USA).

Table 2
Ranges of variables and parameters of the BESS-Rice model.

Variables/ Parameters	Description	Unit	Min	Max
T_a	Atmospheric temperature	K	288	313
T_d	Dew point temperature	K	273	303
WS	Wind speed	$m\,s^{-1}$	0.1	20
PAR	Photosynthetically active radiation	$W\,m^{-2}$	100	500
f_{dif}	fraction of diffuse PAR to global PAR	[−]	0.1	1
LAI	Leaf index area	[−]	0.1	10
$ALB_{WSA-VIS}$	White sky albedo in the visible range	[−]	0.001	0.3
$ALB_{WSA-NIR}$	White sky albedo in the near-infrared range	[−]	0.001	0.6
CI	Clumping index	[−]	0.5	1
$V_{max}^{25°C}$	Peak value of the maximum rice leaf carboxylation capacity at 25 °C over the whole growing season	$\mu mol\ m^{-2}\,s^{-1}$	50	200
ρ_c	Carbon content of a rice plant	[−]	0.2	0.6
φ	NPP/GPP ratio	[−]	0.4	0.9
C_m	Grain moisture content	[−]	0.01	0.2

2.4.1. Satellite data and preprocess

Satellite and reanalysis data derived T_a, T_d, WS, PAR, albedo, CI, LAI, and NDVI were used as forcing variables at all sites. The downscaled T_a and T_d with a spatial resolution of 0.05° were derived from the original 0.5° MERRA reanalysis data (Rienecker et al., 2011) based on the following two equations,

$$X_{fine} = R_{fine} \times C_{fine} \tag{17}$$

$$C_{coarse} = X_{coarse} / R_{coarse} \tag{18}$$

Where X_{fine}, X_{coarse} and R_{fine} are the downscaled (*fine*) MERRA data, original (*coarse*) MERRA data and the MODIS-derived data as reference, respectively. R_{coarse} was aggregated from R_{fine} by averaging fine resolution data within each coarse resolution grid. C is the downscaling coefficient, and C_{fine} was linearly interpolated from C_{coarse}. WS data was derived from the WorldClim 2 datasets (Fick and Hijmans, 2017). The 30′ and monthly mean WS data was aggregated into 0.05° and interpolated into daily.

MODIS atmospheric profile, aerosol, cloud, and albedo products were used to calculate PAR at daily 5 km resolution (Ryu et al., 2018).The daily albedo product MCD43A3(Salomon et al., 2006) and a 500 m monthly mean MCD43A1-based CI product (Wei and Fang, 2016) were applied. Both LAI and NDVI were calculated using the 8 d 250 m MOD09Q1 reflectance product after deleting the records of bad quality (i.e. cloudy) according to the quality control (QC) band. CI, LAI, and NDVI were all interpolated at the daily scale using the smoothing spline in MATLAB®. A comparison of the existing remote sensing LAI products and *in-situ* measurements at CRK in 2015 and 2016 is shown in Fig. A1 in Appendix A. Because of the inaccuracy of LAI products for paddy rice, the empirical relationship between LAI and the near-infrared reflectance of vegetation (NIR_V) (Badgley et al., 2017) was developed using destructive LAI data and FieldSpec® 4 Wide-Res Field Spectroradiometer (Analytical Spectral Devices, Boulder, CO, USA) measured reflectance over the whole growing season in 2015 and 2016 at CRK (Fig. A2 in Appendix A). The detailed information regarding these *in-situ* LAI and reflectance measurements is in Section 2.4.3. According to this empirical relationship, LAI values were estimated using the MOD09Q1 reflectance product for all sites.

2.4.2. Tower-based EC data

For model development and evaluation, EC systems were used to measure CO_2 fluxes at the three sites. The EC systems consist of a three-dimensional sonic anemometer (Model CSAT3, Campbell Scientific Inc., Logan, UT, USA) and an enclosed-path infrared gas analyzer (Model LI-

7200, LI-COR Inc., Lincoln, NE, USA) for CRK and CFK, and a CSAT3 and an open-path infrared gas analyzer (Model LI-7500, LI-COR Inc.) for GRK. The EC instrumentations were mounted on the flux towers at heights of 10, 20 and 5.2 m for CRK, CFK, and GRK, respectively. Other measurements such as net radiation, air temperature, humidity, and precipitation were also conducted at the sites.

To improve the data quality by eliminating undesirable data, the collected data were examined by the quality control (QC) procedure based on the KoFlux data processing protocol (Hong et al., 2009a). After QC, the missing data were gap-filled using a marginal distribution sampling (Reichstein et al., 2005). In terms of nighttime CO_2 flux correction and its partitioning into GPP and ecosystem respiration (RE), the friction velocity (u^*) correction method was applied, with the modified moving point test method for determining u^* threshold (Kang et al., 2017). The nighttime values of RE were extrapolated into the daytime values using the RE equation (Lloyd and Taylor, 1994), with a short-term temperature sensitivity of RE from the nighttime data (Reichstein et al., 2005). The 30 min GPP (μmol CO_2 $m^{-2} s^{-1}$) data were summed into daily GPP (g C m^{-2} d^{-1}). EC-derived GPP values at all sites were used for model evaluation, and EC-derived GPP data at CRK was used for the development of BESS-Rice.

2.4.3. Field measurements of biometric parameters and canopy reflectance

2.4.3.1. Dry mass proportion, phenology and NPP. To develop the dry matter partitioning module of BESS-Rice, *in-situ* dry mass values of all components (leaf, stem, grain, and root) were measured. The same rice plant samples used for destructive LAI analysis were used for the measurement of the dry mass proportion at CRK in 2015 and 2016, respectively. All components were oven-dried at 80 °C for 48 h. The dry matter weight of each component was measured using a CAS CUX-220H laboratory balance (Mettler-Toledo, Columbus, OH, USA), and the dry mass proportion was calculated.

For CRK and CFK, the actual dates of transplanting and harvest were recorded. The approximate start date of booting stages were determined by the weekly observation, when there was bulging of the leaf stem that conceals the developing panicle. For GRK, the information of phenology was obtained from the literature (Kim et al., 2016; Min et al., 2013). The dates of transplanting and harvest were used to determine the onset and end of rice growing season. Measurements of starts of booting stage at CRK were used to determine the threshold of $GPP_{norm-accu}$ for detecting this stage. Dates of booting stage at CFK and GRK were used for evaluation.

The total rice plant net primary production (NPP_t) value at harvesting in 2016 was calculated using the following equation (Huang et al., 2007; Lobell et al., 2002).

$$NPP_t = W_t \times C \quad (19)$$

where W_t is the total (including aboveground and belowground parts) dry mass (g m^{-2}) of a rice plant; and C is the carbon content of a rice plant, which was set to 0.4 according to the carbon content values of different components measured at CRK in 2015. The NPP value was also obtained in 2016 for CFK based on six samples and using the same strategy. NPP data at GRK in 2012 was obtained from the literature (Min et al., 2013). NPP data was used to develop the dry matter accumulation module of BESS-Rice.

2.4.3.2. Yield and grain moisture. For the evaluation of BESS-Rice yield, mature rice panicles were sampled at nine random points using a 0.25 × 0.25 m^2 plot at CRK in 2015 and 2016 and CFK in 2016; and at three random points using a 3.3 m^2 plot at GRK in 2011, 2012, and 2014. After threshing, the grain (brown rice with chaff) weight values were measured after air-drying until a constant weight was reached. For CRK and CFK, grain dry weight values were measured after oven-drying and grain moisture was calculated, while for GRK, a grain moisture meter was used. Finally, per unit area grain yield values were calculated based on the stem density. All yield, stem density and grain moisture values are listed in Table 1.

2.4.3.3. Canopy spectral reflectance. To build the MODIS reflectance-based LAI estimation model, a ground-based rice canopy spectral reflectance was measured using a FieldSpec® 4 Wide-Res Field Spectroradiometer at CRK in 2015 and 2016 (Table A1 in Appendix A). The spectroradiometer had a full width at half maximum (FWHM) of 3 nm and a sampling interval of 1.4 nm between 350–1000 nm. A 25° field of view was used and the fiber optic was placed about 1 m above the rice canopy. All spectral radiance data was measured under relatively cloud-free and stable sky conditions between 10:00 and 14:00 (local solar time). Spectralon® Diffuse Reflectance Standards (Labsphere, North Sutton, NH, USA) was used under the same illumination conditions to convert the radiance to spectral reflectance. Mean spectral reflectance was determined from 25 samples at every visit.

2.4.3.4. LAI. To build the remote sensing LAI estimation model, the LAI was measured at CRK. A total of three and six destructive samples (one sample included a hill of rice plants) were collected around the tower in 2015 and 2016, respectively (Table A1 in Appendix A). Leaves from the samples were affixed on a white panel using transparent tape and scanned to obtain digital images with 300 dpi. The digital images were segmented into five classes using the k-means algorithm, and the classes that indicated leaves were selected based on a visual interpretation to exclude the background noise. The average leaf area per sample was then calculated. LAI values were calculated in terms of the leaf area per sample (hill) and rice hill density per m^2.

3. Results

3.1. Evaluation of simulated GPP

Overall, the BESS-Rice simulated GPP had a seasonal pattern consistent with that of EC-derived GPP estimates at the daily scale (Fig. 4). In all site years (Fig. 5), BESS-Rice explained 62%–86% of seasonal variation in EC-derived GPP estimates. The RMSE ranged from 1.8 g C m^{-2} d^{-1} (relative RMSE = 25.8%, CRK in 2016) to 2.7 (33.4%, GRK in 2011) g C m^{-2} d^{-1}. The bias varied from –0.7 g C m^{-2} d^{-1} (relative bias = −9.3%, CRK in 2016) to –1.1 (–14.0%, GRK in 2011) g C m^{-2} d^{-1}. The average RMSE value of simulated and measured daily GPP was 2.2 g C m^{-2} d^{-1} (29.5%), with a bias value of –0.5 g C m^{-2} d^{-1} (–7.1%). The largest negative differences between GPP derived from BESS-Rice and the EC-measured GPP occurred in the early stages (in the 17 and 28 days after transplanting in 2015 and 2016, respectively) at CRK with a relative bias less than –60%. The largest positive differences between modelled and EC-derived values appeared in less than 10 days before harvest at CRK and CFK with a relative bias larger than 50%. A site-by-site comparison of the simulated and EC-based maximum of accumulated GPP ($GPP_{max-accu}$) over the whole growing season is shown in Table 3. All the simulated $GPP_{max-accu}$ values were underestimated, and the bias varied from –28.4 (–3.4%, CRK in 2016) to –136.6 (–14.1%, GRK in 2011) g C m^{-2}. The average RMSE values of simulated and measured $GPP_{max-accu}$ at all sites was 75.2 (8.7%), while the bias was –65.9 (–7.7%). To calculate $GPP_{norm-accu}$ in the previous years, $GPP_{max-accu}$ in each year was used in this study. For applying BESS-Rice during the current year growing season (i.e. before the harvest), the multi-year mean BESS derived $GPP_{max-accu}$ could be used. Using a fixed onset and end of rice growing season for each site averaged from the available data, we simulated $GPP_{max-accu}$ from 2000 to 2016 at CRK, CFK and GRK. Correspondingly, the average $GPP_{max-accu}$ values were 788.09 (± 22.48) g C m^{-2}, 831.12 (± 23.93) g C m^{-2}, and 913.16 (± 28.96) g C m^{-2}, respectively. The average surveyed rice yields (obtained from Korean Statistical Information Service, http://kosis.kr/) of the counties, where CRK, CFK and GRK are located, from 2000 to 2016 were 6948.83 (± 238.21)

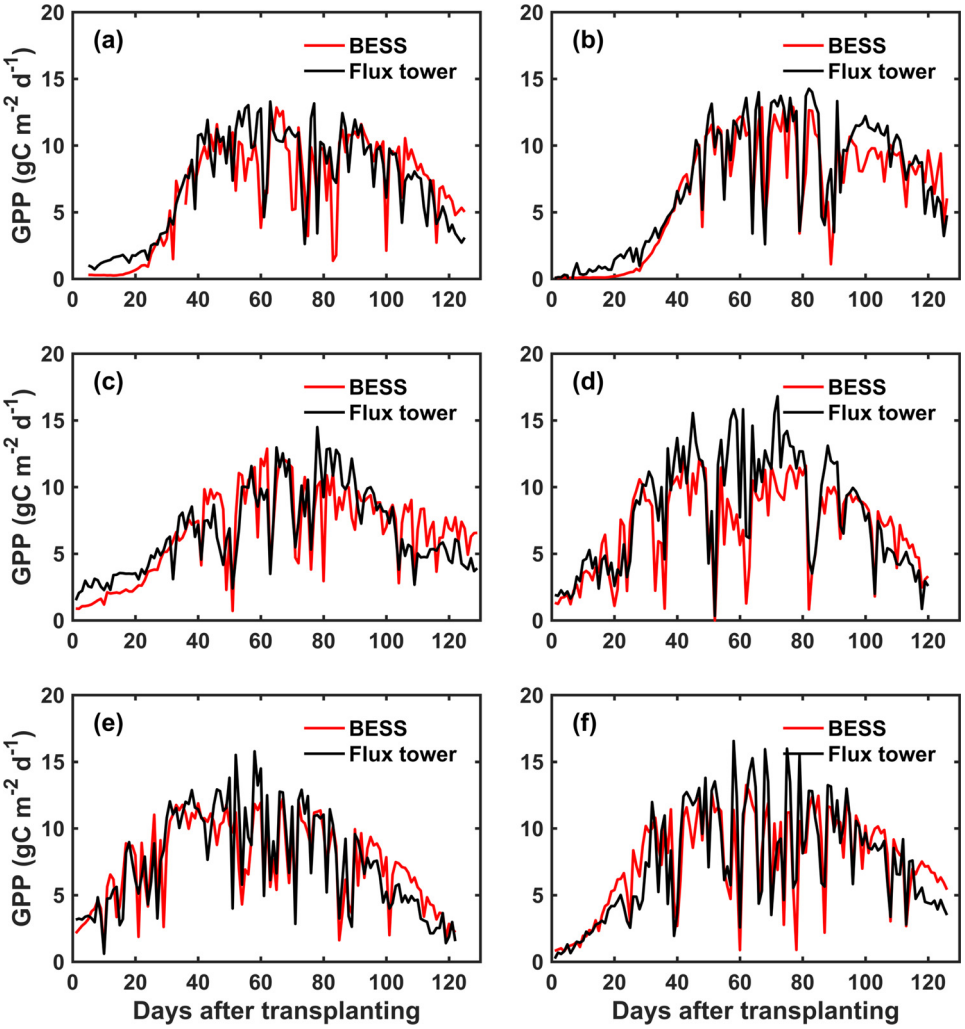

Fig. 4. Seasonal dynamics of simulated and flux tower-based EC data derived daily GPP during rice growing seasons. (a) CRK in 2015, (b) CRK in 2016, (c) CFK in 2016, (d) GRK in 2011, (e) GRK in 2012, and (f) GRK in 2014.

kg ha^{-1}, 6329.05 (± 197.69) kg ha^{-1} and 7209.18 (± 198.60) kg ha^{-1}, respectively. The inter-annual variation of the multi-year mean BESS derived $GPP_{max-accu}$ was 3.0%, which was consistent with the inter-annual variations (3.1%) of surveyed yield.

3.2. Evaluation of the simulated phenological phase and dry mass proportion

BESS-Rice simulated $GPP_{norm-accu}$ values were highly linearly related with the EC-derived $GPP_{norm-accu}$ values. As shown in Table 4, over 99.8% variations of EC-derived $GPP_{norm-accu}$ values could be explained by BESS-Rice simulated estimates. The RMSE ranged from 0.01 (2.6%, GRK in 2012) to 0.05 (11.7%, CRK in 2015). The bias varied from –0.01 (–1.6%, GRK in 2012) to − 0.05 (10.5%, CRK in 2015). The average RMSE value of simulated and measured daily $GPP_{norm-accu}$ was 0.03 (6.9%), with a bias value of –0.02(–4.0%).

BESS-Rice derived start dates of booting stage could explain 76% variations of actual beginnings of booting stages at CFK and GRK over the different years, with a RMSE value 4.7 d (8.3%) and bias value –3.8 d (–6.6%). The site-by-site analysis (Table 4) showed that the bias varied from –8 d (–15.1%, GRK in 2012) to 0 d (0%, GRK in 2011).

BESS-Rice derived dry matter partitioning coefficient values, which differ from the EC-derived GPP used to build Eqs. (4)–(7), agreed well with the seasonal trajectory of field measurements at CRK in 2015 and 2016. The exception is the mid-stage (between 65 and 90 days after transplanting) for leaf in 2015 and the early stages (15 days after transplanting) for leaf and stem in 2016 (Fig. 6). As shown in Table 5, the average RMSE values were 0.05 (24.1%), 0.06 (20.3%), 0.06 (11.2%) and 0.09 (26.5%), and bias values were 0.01 (4.6%), 0.02 (5.0%), 0.01 (2.8%), –0.05 (–15.2%) for leaves, stems, grains and belowground components, respectively.

3.3. Evaluation of simulated yield againstin-situ measurements

BESS-Rice simulated yield could explain over 82% of the variations in field measured yield at the different sites and over the different years (Fig. 7), with a RMSE of 534.8 kg ha^{-1} (7.7%) and bias of 242.1 kg ha^{-1} (3.5%). The site-by-site analysis (Table 6) showed that BESS-Rice derived yield values were underestimated at GRK in 2011 and 2014 with the bias values of –524.6 kg ha^{-1} (–8.0%) and –275.4 kg ha^{-1}(–3.9%). BESS-Rice overestimated yield at the other site-year, with the bias varied from 340.5 kg ha^{-1}(5.7%, CFK in 2016) to 754.0 kg ha^{-1}(13.2%, GRK in 2012).

3.4. Sensitivity analysis of BESS-rice

The SA between the BESS-Rice simulated GPP and the forcing variables (T_a, T_d, WS, PAR, f_{dif}, LAI, $ALB_{WSA-VIS}$, $ALB_{WSA-NIR}$, CI and peak $V_{max}^{25°C}$) (Fig. 8a) showed that LAI and PAR were the most sensitive forcing variables in simulating daily GPP, with total-order sensitivity

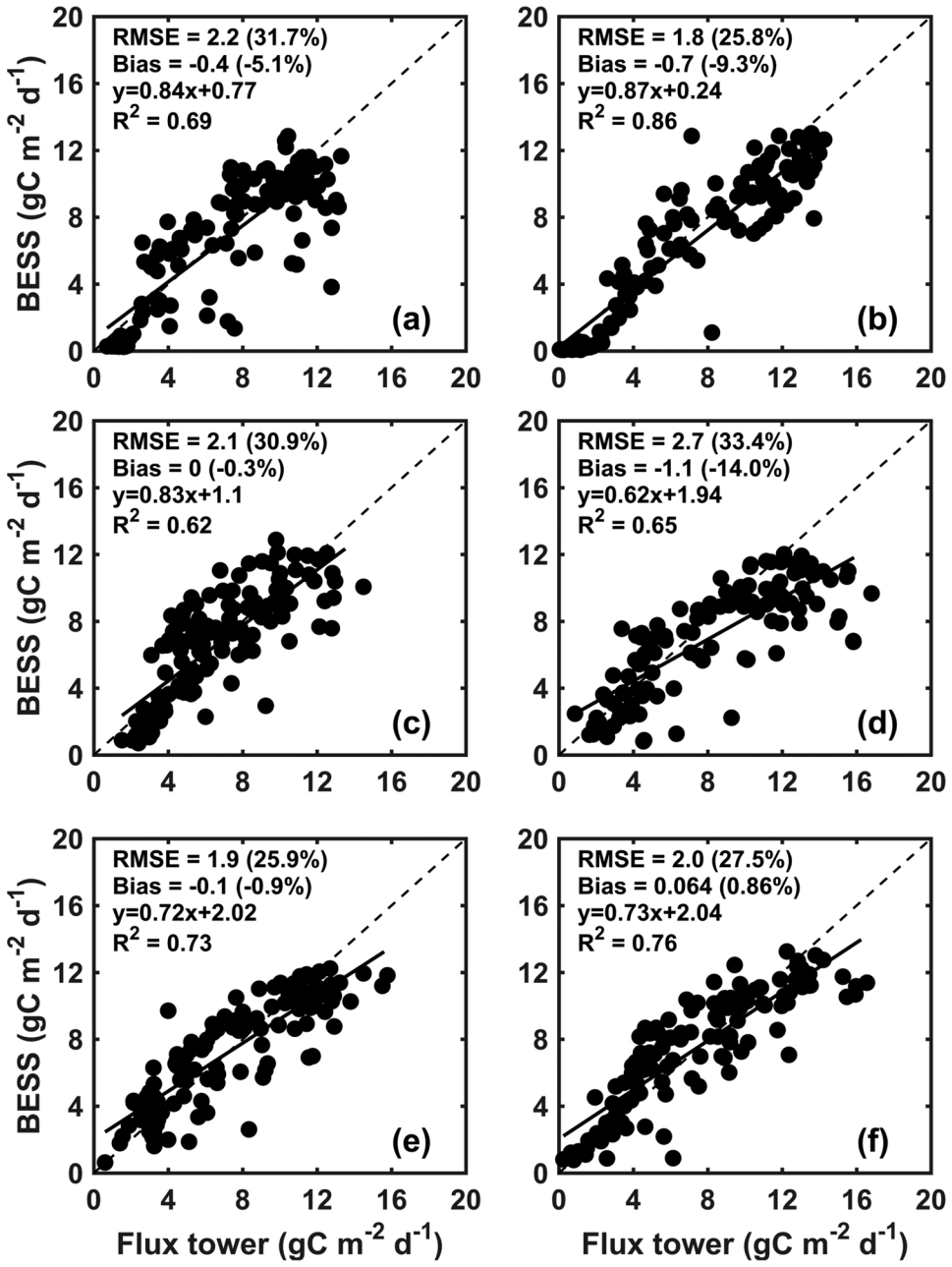

Fig. 5. Comparison of simulated and flux tower-based EC data derived daily GPP during rice growing seasons. (a) CRK in 2015, (b) CRK in 2016, (c) CFK in 2016, (d) GRK in 2011, (e) GRK in 2012, and (f) GRK in 2014. Solid lines are trend lines and dash lines are 1:1 lines.

Table 3
Comparison of the simulated and *in-situ* measured maximum accumulated gross primary product (GPP).

Site	Year	Simulated $GPP_{max-accu}$ ($g\,C\,m^{-2}$)	Measured $GPP_{max-accu}$ ($g\,C\,m^{-2}$)	Bias	Relative bias (%)
CRK	2015	811.79	855.54	−43.74	−5.11
	2016	810.49	838.86	−28.37	−3.38
CFK	2016	855.56	905.49	−49.93	−5.51
GRK	2011	835.71	972.32	−136.61	−14.05
	2012	898.63	985.24	−86.61	−8.79
	2014	943.75	994.08	−50.34	−5.06

index (S_T) of ~40%. T_a was the third most sensitive variables, with S_T of 26%. Peak $V_{max}^{25°C}$, $ALB_{WSA-VIS}$, T_d, f_{dif}, WS, CI and $ALB_{WSA-NIR}$ were relatively insensitive forcing variables, with S_T less than 10%.

In terms of the SA between the BESS-Rice simulated yield and the forcing variables (T_a, T_d, WS, PAR, $f_{PAR.diff}$, LAI, $ALB_{WSA-VIS}$, $ALB_{WSA-NIR}$, CI and peak $V_{max}^{25°C}$) and input parameters (φ, ρ_c, and C_m), the results (Fig. 8b) showed that LAI and PAR were also the most sensitive forcing variables to simulate yield, which governed over 30% and 29% of variations in yield, respectively. T_a was also the third most sensitive forcing variables, with S_T of 19%. In addition, BESS-Rice simulated yield was sensitive to the input parameters ρ_c and φ, with S_T of 25% and 13%. Peak $V_{max}^{25°C}$, $ALB_{WSA-VIS}$, f_{dif}, C_m, T_d, WS, CI and $ALB_{WSA-NIR}$ were relatively insensitive variables and parameters to simulated yield, with the S_T values less than 5%.

Table 4
Comparison of the simulated and *in-situ* measured normalized accumulated gross primary productivity ($GPP_{norm-accu}$) and the start of booting stage.

Site	Year	$GPP_{norm-accu}$					Start of booting stage	
		RMSE	Relative RMSE (%)	Bias	Relative bias (%)	R^2 ($p < 0.01$)	Bias (d)	Relative bias (%)
CRK	2015	0.05	11.73	−0.05	–10.47	0.998	5	8.47
	2016	0.02	4.91	–0.02	–3.85	0.999	1	1.52
CFK	2016	0.03	7.41	–0.03	–6.28	0.998	–4	–6.15
GRK	2011	0.04	7.26	–0.02	–4.57	0.997	0	0.00
	2012	0.01	2.64	–0.01	–1.59	0.999	–8	–15.09
	2014	0.02	3.88	0.01	2.29	0.999	–3	–5.26

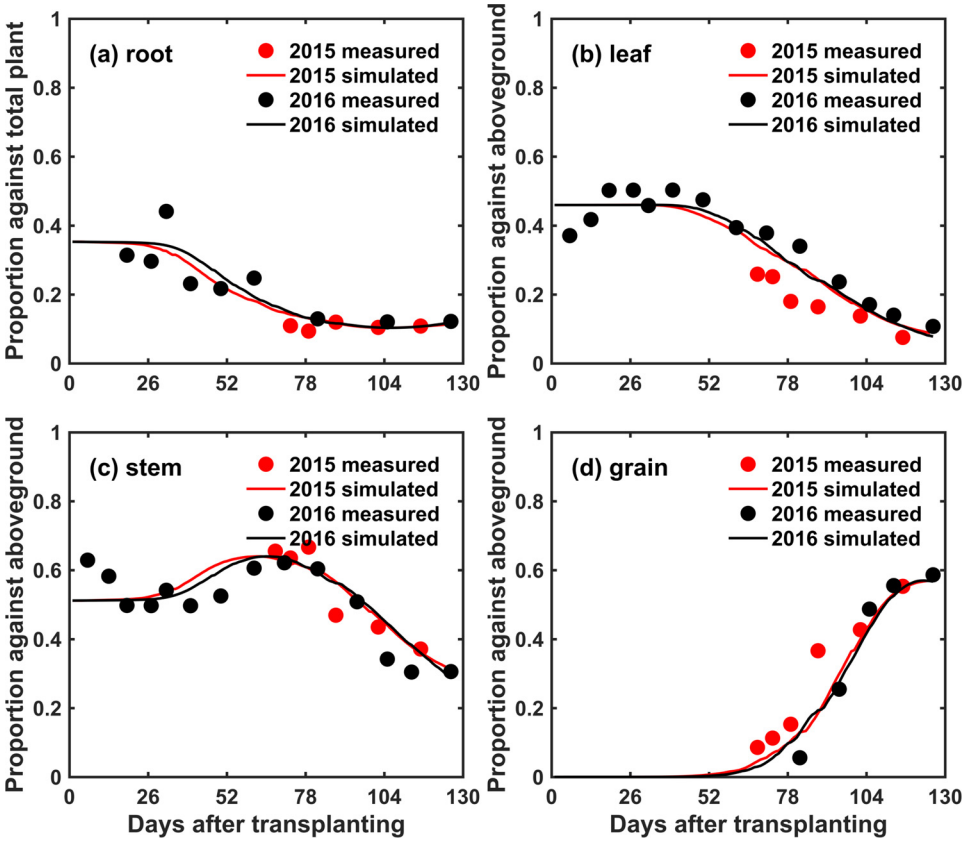

Fig. 6. Comparison of the simulated and *in-situ* measured dry mass proportion of different components during rice growing seasons at CRK in 2015 and 2016. (a) Dry mass proportion of belowground parts (root) against the whole plant, (b) dry mass proportion of leaves against aboveground parts, (c) dry mass proportion of stems against aboveground parts, and (d) dry mass proportion of grain against aboveground parts.

Table 5
Comparison of the simulated and *in-situ* measured dry mass proportion of different components at CRK in 2015 and 2016.

Year	Component	RMSE	Relative RMSE (%)	Bias	Relative bias (%)
2015	root	0.03	25.76	0.02	16.65
	leaf	0.09	52.12	0.09	48.73
	stem	0.06	10.83	0.02	3.79
	grain	0.11	39.42	–0.09	–31.86
2016	root	0.05	22.59	0.00	1.55
	leaf	0.04	11.64	–0.02	–4.37
	stem	0.06	11.34	0.01	2.36
	grain	0.05	11.49	0.00	–0.66

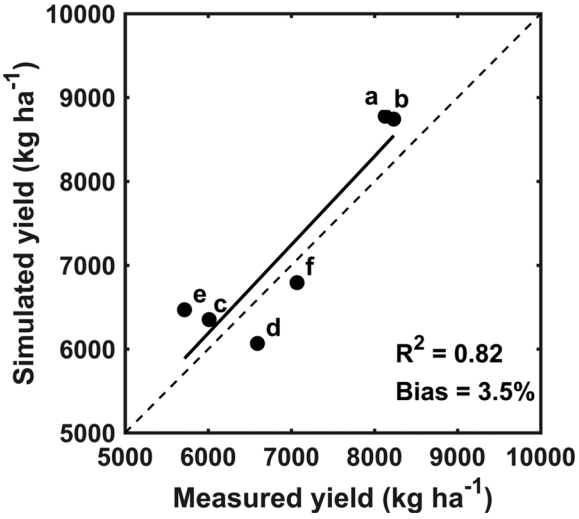

Fig. 7. Comparison of simulated and *in-situ* measured rice grain yields. (a) CRK in 2015, (b) CRK in 2016, (c) CFK in 2016, (d) GRK in 2011, (e) GRK in 2012, and (f) GRK in 2014. Solid line is trend line and dash line is 1:1 line.

4. Discussion

4.1. General performance and advantages of BESS-rice

BESS-Rice could capture most of the seasonal variations of EC-derived GPP (Fig. 4). The simulated $GPP_{norm-accu}$ values were closely related with the EC-derived $GPP_{norm-accu}$ values (Table 4). It indicated that the biases in BESS-Rice derived GPP were not propagated into the linear

Table 6
Comparison of the simulated and *in-situ* measured yield.

Site	Year	Bias (kg ha^{-1})	Bias (%)
CRK	2015	648.12	7.97
	2016	510.16	6.20
CFK	2016	340.54	5.67
GRK	2011	–524.63	–7.96
	2012	753.98	13.19
	2014	–275.37	–3.90

relationship in $GPP_{norm-accu}$ between BESS-Rice and EC. The small inter-annual variations of the multi-year mean BESS derived $GPP_{max-accu}$ were consistent with the inter-annual variations of surveyed yield, and it demonstrated the feasibility of using the multi-year mean BESS derived $GPP_{max-accu}$ in estimating current year rice growth situations. BESS-Rice performed well in terms of yield estimation across all three sites during the different years (Fig. 7). This indicates that BESS-Rice could capture the spatial gradients of rice productivity, and has the potential for regional application. The conventional rice simulation models, CERES-Rice had relative RMSE values from 3% to 32% (averagely 23%) against the *in-situ* measurements across a range of experiments in Asia and Australia (Timsina and Humphreys, 2006); ORYZA2000 had a relative RMSE value of 8.4% against the measured yield at one site in India (Li et al., 2013), and had same relative RMSE values of 13% against the observed yield under different irrigation regimes at two sites in China and Philippines (Belder et al., 2007). In terms of agro-land surface model, MATCRO-Rice had a 4-year mean relative RMSE value of 8.1% against the *in-situ* measurements in Japan (Masutomi et al., 2016b). The previous researches showed the rice simulation models performed satisfactorily with relative RMSE values less than 10%. BESS-Rice achieved relative RMSE less 10% with much fewer forcing variables and parameter calibration.

Due to the limitations in obtaining dry mass data for each rice component, dry matter partitioning coefficients were only simulated at one site during two years (Fig. 6). We found that BESS-Rice performed well in the dry matter partitioning dynamic simulation, which was expected as BESS-Rice simulated GPP well captured seasonality of EC-derived GPP. Further extensive evaluation of dry matter partitioning should be conducted in different rice production areas and different years. In most crop simulation models and agro-land surface models, dry matter partitioning is based on fixed partitioning coefficients that may additionally depend on development stages of the crop (Priesack and Gayler, 2009; Xia et al., 2017). For example, in JULES-SUCROS (Van den Hoof et al., 2011), the allocation of dry matter over the various plant organs was described by fixed distribution factors which depended on the development stage, and the values for these factors were taken from Penning de Vries et al., 1989. For evaluation of dry matter partitioning, few studies directly used the *in-situ* seasonal partitioning coefficients over the different components (especially, root). Therefore, the seasonal partitioning coefficients data used in this study is valuable for the further assessment and application of the carbon allocation-based models.

In conventional crop models, the state variables that quantify the effects of temperature and photoperiod on crop growth are usually used to indicate the crop development rate and simulate the phenology of crop growth, e.g., growing degree days (GDD) (Ritchie et al., 1998), physiological development time (PDT) (Cao and Moss, 1997; Tang et al., 2009), and development stage (DS) (Fumoto et al., 2008; Sus et al., 2010). In this study, $GPP_{norm-accu}$ which represents photosynthetic activation and is more directly related to rice growth situations (e.g., dry mass accumulation), was used as a scaler to quantify the rice development rate. Fig. A1 in Appendix A shows that over 94% of the variations in the dry matter partitioning coefficients of rice grains could be explained by EC-derived $GPP_{norm-accu}$, and over 93% of the variations in dry matter partitioning coefficients of rice grains could be explained by the tower-based T_a derived GDD. This indicated that $GPP_{norm-accu}$ agreed well with the GDD in dry matter partitioning dynamics and could be used to replace GDD for rice development simulation. In addition, BESS-Rice simulated $GPP_{norm-accu}$ also had a similar performance with MERRA derived GDD in grain dry matter partitioning coefficients estimation. This revealed again that the uncertainty in GPP simulations did not propagate in dry matter partitioning coefficients estimation after the normalization of GPP. GPP is the total amount of carbon dioxide that is fixed by plants in photosynthesis, and it is also closely related to the crop physiological indices, such as chlorophyll (Gitelson et al., 2006; Peng et al., 2013). Therefore, theoretically, the remote sensing-derived $GPP_{norm-accu}$ is more directly related to rice growth conditions and might enable us to reduce the uncertainty related to other environmental variables while detecting key processes. BESS-Rice simulated $GPP_{norm-accu}$ performed well in detecting the start of the booting stage with an average RMSE of 4.7 d and relative bias of –3.8 d, using a simple empirical approach with minor requirements of priori agronomic expert knowledge. For the meteorological factors-based indicators, more physiological mechanism of crop growth must be considered when they are used to determine the crop growth stages (Tang et al., 2009).

Compared with the conventional process-based crop models (e.g., APSIM-ORYZA, CERES-Rice, and DNDC-Rice) and agro-land surface models [e.g., JULES- SUCROS (Best et al., 2011; Clark et al., 2011; Van den Hoof et al., 2011), and ORCHIDEE-Crop (Wu et al., 2016)], BESS-Rice is highly simplified and could be easier to be applied regionally.

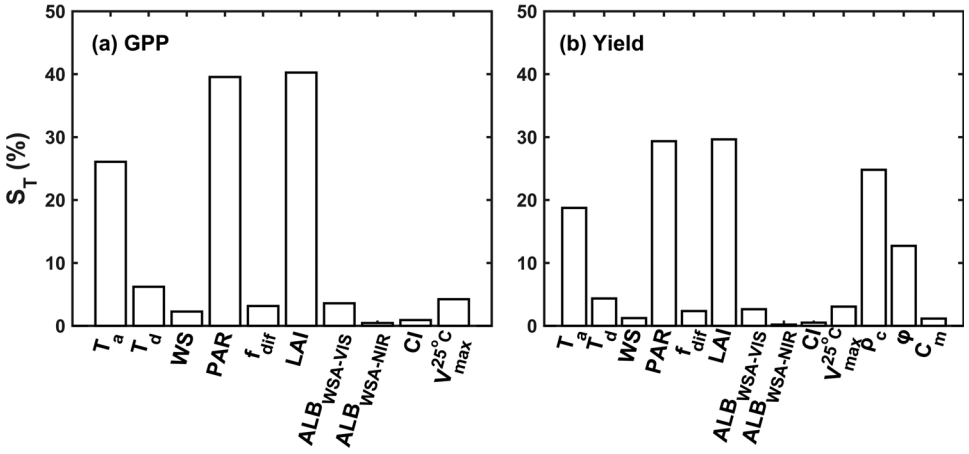

Fig. 8. Sensitivity analysis of BESS-Rice. Total sensitivity index (S_T) of variables and parameters for (a) GPP and (b) yield. T_a, atmospheric temperature; T_d, dew point temperature; WS, wind speed; PAR, photosynthetically active radiation; f_{dif}, fraction of diffuse PAR to global PAR; LAI, leaf index area; ALBWSA-VIS, white sky albedo in the visible range; ALBWSA-NIR, white sky albedo in the near-infrared range; CI, clumping index; $V_{max}^{25°C}$, peak value of the maximum rice leaf carboxylation capacity at 25 °C over the whole growing season; ρ_c, carbon content of a rice plant; φ, NPP/GPP ratio; C_m grain moisture content.

This is because BESS-Rice requires far fewer forcing variables (Table A1 in Appendix A) than the conventional models, and all the variables can be derived from airborne or satellite data and reanalysis data. For instance, ORYZA-2000 model, which derives APSIM-ORYZA model, requires dozens of soil properties for paddy including physical and chemical characteristics such as soil type, composition, texture, water storage capacity, bulk density, and pH; dozens of cultivation management including phenological stages, irrigation, fertilizer application, planting distance and density; and similar numbers of weather variables as BESS-Rice requires (Bouman et al., 2001). Neither soil property nor agronomical management data are normally be unavailable at regional scale. However, based on the remote sensing retrieved biophysical state variables, the uncertainty that is probably caused by the unavailability of soil properties, crop varieties, and cultivation management might be lessened. Moreover, due to the simplicity of model development, BESS-Rice could be easily extended and applied to other crop types. BESS-Rice is a diagnostic model based on the remote sensing-derived forcing variables. The rice growth status which directly related to irrigation, fertilizer and other management practices, could be identified from these remote sensing derived variables, such as LAI.

Compared with the empirical remotely sensed productivity estimation methods, e.g., the HI based estimation method (Yuan et al., 2016), the process-based BESS-Rice model can reveal the rice growth process, especially the dry matter allocation dynamic among the different components at different phrases (Fig. A2 in Appendix A), which is strong related to yield formation and environmental factors, e.g., temperature, and radiation. (Kim et al., 2011; Okawa et al., 2003). Such a process-oriented approach enabled us have the possibility to investigate what controls and impacts the final yield formation, and when such impacts occur. The dynamic simulations could be used to provide information for agronomic diagnoses, and to study the rice yield production response to climate change. Besides, BESS-Rice coupled the Farquhar photosynthesis model (Farquhar et al., 1980) and Penman-Monteith evaporation model (Monteith, 1965), so the relationships between the simulations and the environmental factors are explicit.

4.2. Uncertainties and limitations of BESS-rice

BESS-Rice derived GPP and yield were most sensitive to LAI and PAR, with S_T of 40% and approximately 30%, respectively. LAI was the most important variable that controlled canopy radiative transfer (Mousivand et al., 2014; Verrelst et al., 2015) and one of the most significant variables that interpret crop growth conditions (Dente et al., 2008; Xie et al., 2017); however, substantial inconsistencies among global LAI products were reported(Jiang et al., 2017). We found that both MODIS and Geov1 LAI products substantially underestimated LAI at the paddy rice sites (Fig. A3 in Appendix A). The underestimation of the current satellite LAI products in cereal crops was also reported in previous studies (Fang et al., 2012; Yang et al., 2007). Based on the two-band (red and near-infrared) 250 m MODIS product, NIR_V (Fig. AFigure 4a) was calculated to estimate LAI in this study, which was linearly related with LAI than NDVI ($R^2 = 0.9$) (Fig. AFigure 2b). As shown in Fig. A4, NDVI was obviously influenced by the background during the early stages (Thenkabail et al., 2000) and was saturated when the canopy coverage was high (Sims and Gamon, 2002). The LAI estimation equation was developed using 2 year *in-situ* measurements at one site. Further extensive evaluation and improvement of this LAI estimation model should be conducted regionally. PAR also drives a multitude of processes related to biosphere-atmosphere interactions. The PAR data used in this research has an accuracy R^2 of 0.94 and relative bias of 1.7% compared with *in-situ* measurements (Ryu et al., 2018). T_a was the second most sensitive variable to simulate both GPP and yield, with S_T between 10% and 30%. As shown in Fig. A5 in Appendix A, MERRA-derived snapshot T_a kept consistent with *in-situ* measured T_a at the different sites and over the different years, with relative RMSE values less than 1%. Therefore, PAR and T_a derived uncertainty of BESS-Rice simulations could be relatively minor.

In terms of the input parameters, ρ_c and φ had relatively high contribution to BESS-Rice simulated yield, with S_T of 25% and 13%. Therefore, the inaccuracy associated with ρ_c and φ could be another main source of uncertainty in BESS-Rice. The seasonal variation of ρ_c was small according to the *in-situ* data. In a similar study, Sus et al. (2010) also used fixed carbon content to convert accumulated carbon into dry mass. However, due to the limitation of both measured and literature-based data, the spatial variation of ρ_c was not studied in this study. In addition, Gifford (1995) proved the constancy of carbon use efficiency (i.e. φ), and therefore a constant φ over whole growing season was viewed as a robust approach to carbon balance modelling. However, φ is highly variable across species, and even for the same species it can vary through time and under different environmental conditions (Guan et al., 2016). There was also a large spatial variation of φ over the three sites used in this study, with φ values varied from 0.50 to 0.79. Therefore the spatial variation of φ should be considered when BESS-Rice model is used for a large area. The spatial pattern of φ could be derived based on the surveyed rice yield-based NPP measures (Guan et al., 2016) and simulated GPP.

In addition, the maximum accumulated GPP over the whole growing season was significant for the simulation of rice development and dry matter partitioning because it was used to calculate $GPP_{norm-accu}$. An accurate extraction of the onset and end of the growing season is important for the calculation of the maximal accumulated GPP, which is critical for extending the present site level BESS-Rice to the regional scale. It is also important for interpreting the inter-annual variability of GPP (Zhou et al., 2016) and capturing the inter-annual variation of yield. The spatial pattern of rice phenological dates, such as the irrigation starting date, transplanting date, and harvest date, could be derived by detecting the key transition features of the time series of remotely sensed vegetation indices or simulated GPP pixel by pixel (Eklundh and Jönsson, 2016; Setiyono et al., 2018). The relationships between $GPP_{norm-accu}$ and dry matter partitioning coefficients were constructed based on 2 year *in-situ* measurements at one site, because simultaneous EC and dry mass data for different rice components (especially roots) were unavailable at the other sites. The relationships between $GPP_{norm-accu}$ and dry matter partitioning coefficients could be impacted by the meteorological conditions, rice varieties, and management practices. Although the accuracy of yield simulations based on the current BESS-Rice model at other sites distributed in South Korea is acceptable, the regional application of BESS-Rice required further evaluation.

5. Conclusion

The remote sensing-derived and biophysical process-based rice productivity simulation model, BESS-Rice, was developed in this study by integrating a rice dry matter partitioning module into the BESS model. Comparisons of simulated GPP, $GPP_{norm-accu}$, start of booting stage and dry mass proportion against field measurements made at site level showed that BESS-Rice performed well in capturing the seasonal pattern of phase development, assimilate accumulation and partitioning over the paddy rice growing season. BESS-Rice also performed well in rice grain estimation, with a RMSE of 534.8 kg ha^{-1} (7.7%) and bias of 242.1 kg ha^{-1} (3.5%). BESS-Rice is much simpler than conventional crop simulation models and could reveal the rice growth process with remote sensing derived forcing variables. This will decrease the uncertainty related to the forcing variables and enable regional application. The model is also expected to provide information for agronomic diagnoses and the potential impacts of climate change on rice productivity. BESS-Rice could contribute advancing integration of remote sensing information and agro-land surface model.

Acknowledgments

This work was funded by the KMA Research and Development Program under the Grant Weather Information Service Engine (WISE)

project (KMIPA-2012-0001-2) and Research Program for Agricultural Science & Technology Development (Project No. PJ01229301), National Institute of Agricultural Sciences, Rural Development Administration, Republic of Korea. We thank Prof. Eunwoo Park for supporting this project. We thank Prof. Joon Kim for envisioning KoFlux, which enabled us to evaluate BESS-Rice. The authors are grateful to all members of the Environmental and Ecology Lab at Seoul National University for assistance with fieldwork.

Appendix A

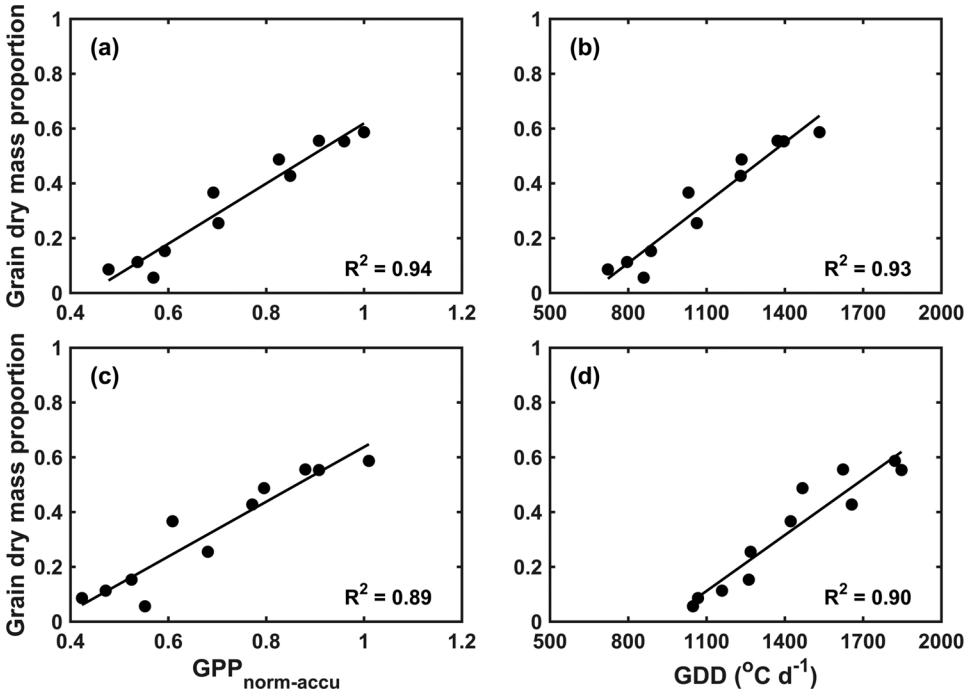

Fig. A1. Comparison of the linear relationships between (a) EC-derived $\mathbf{GPP_{norm-accu}}$, (b) Tower-based growing degree days (GDD), (c) BESS-Rice derived $\mathbf{GPP_{norm-accu}}$ and (d) MERRA T_a derived GDD and the dry matter partitioning coefficient of grain at CRK in 2015 and 2016. Solid lines are trend lines.

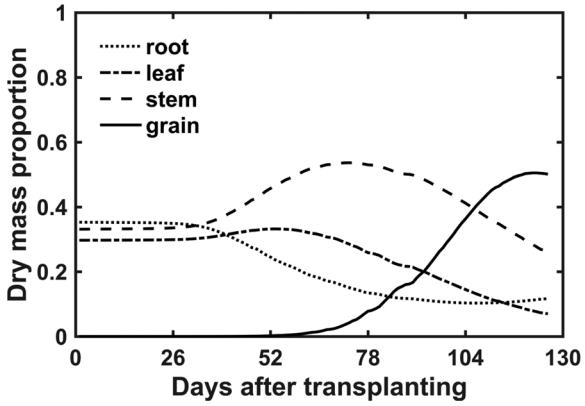

Fig. A2. Simulated dry mass proportion of different components against the whole rice plant during growing seasons at CRK in 2016.

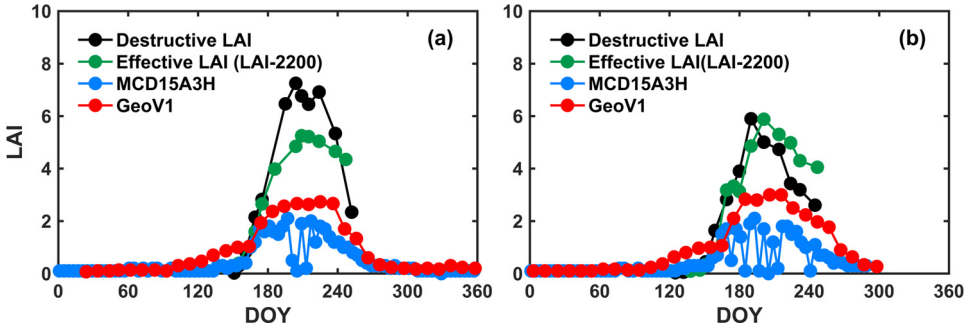

Fig. A3. Comparison of satellite LAI production and *in-situ* measurements at CRK in (a) 2015 and (b) 2016.

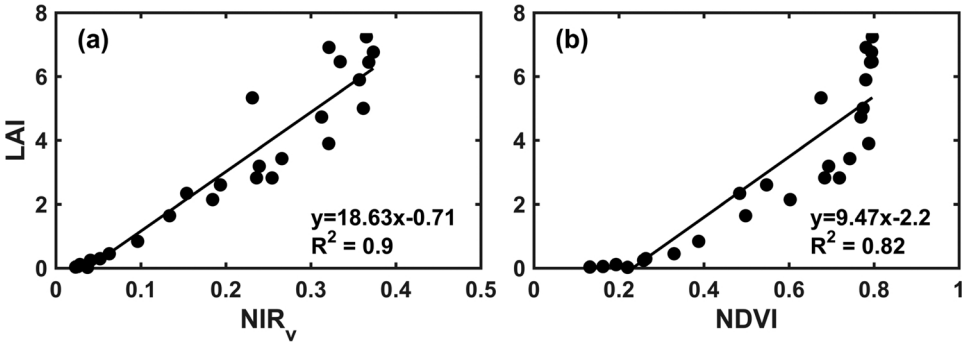

Fig. A4. Leaf area index (LAI) estimation function based on (a) the near-infrared reflectance of vegetation (NIR_V) and (b) Normalized Difference Vegetation Index (NDVI). Data is from *in-situ* measured LAI data at Cheorwon Rice paddy KoFlux site (CRK) and MOD09Q1 reflectance products in 2015 and 2016. Solid lines are trend lines.

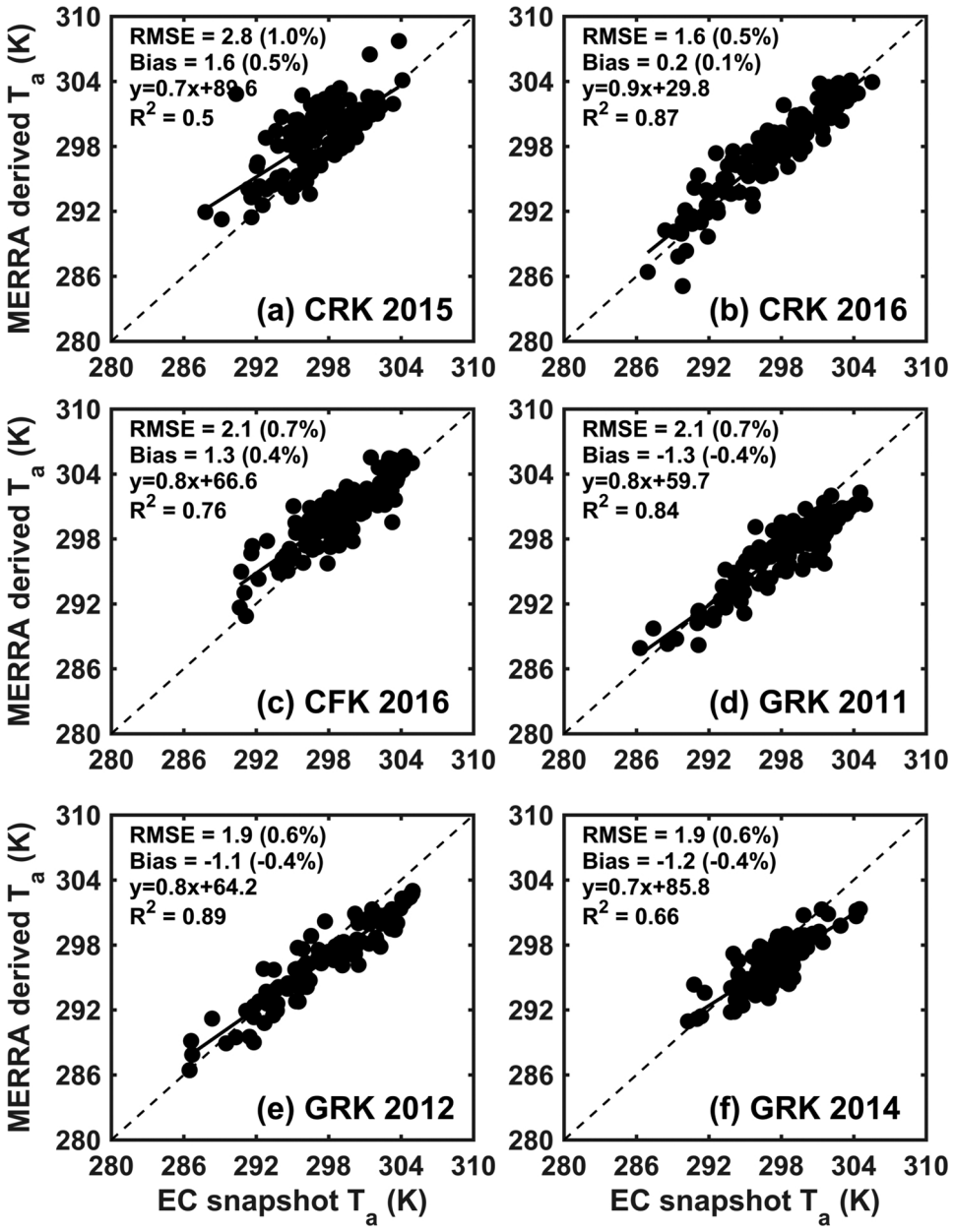

Fig. A5. Comparison of the EC derived snapshot and the MERRA derived T_a at CRK, CFK and GRK. Dash line is 1:1 line.

Table A1
Information list of data used in this research.

Symbols	Description	Data source	Spatial resolution	Frequency/ Measuring date	Data covering period	Data use
		Satellite/reanalysis products (all sites)				
T_a	Atmospheric temperature (K)	downscaled MERRA reanalysis data (Rienecker et al., 2011)	0.05°	Daily	Whole growing season	BESS-Rice forcing variables
T_d	Dew point temperature (K)	downscaled MERRA reanalysis data(Rienecker et al., 2011)	0.05°	Daily	Whole growing season	
WS	Wind speed (m s^{-1})	interpolated WorldClim 2 (Fick and Hijmans, 2017)	0.05°	Monthly to Daily	Whole growing season	
PAR	Photosynthetically active radiation (W m^{-2})	Calculated from MODIS atmospheric profile, aerosol, cloud, and albedo products (Ryu et al., 2018)	5 km	Daily	Whole growing season	
LAI	Leaf index area	Estimated from MOD09Q1 reflectance based on the linear relationship between the destructive LAI and NIRv	250 m	8d to Daily	Whole growing season	
LAI	Leaf index area	Destructive LAI (CRK)	*in-situ*	Daily	DOY 151, 155, 161, 169, 175, 195, 204, 209, 215, 224, 238, and 252 in 2015; DOY 125, 132, 138, 146, 151, 159, 169, 180, 190, 201, 214, 224, 232, and 245 in 2016.	
Ref	Reflectance	Measured by FieldSpec® 4 Wide-Res Field Spectroradiometer	*in-situ*	Daily	DOY 155, 161, 169, 175, 195, 204, 215, 224, 238, and 247 in 2015; DOY 125, 132, 138, 146, 151, 159, 169, 180, 190, 201, 214, 224, 232, and 245 in 2016	
ALB_WSA_VIS	White sky albedo in the visible range	MCD43A3 albedo product	500 m	Daily	Whole growing season	
ALB_WSA_NIR	White sky albedo in the near-infrared range		500 m			
CI	Clumping index	interpolated Clumping index products based on MCD43A1 (Wei and Fang 2016)	500 m	Monthly to Daily	Whole growing season	
NDVI	Normalized difference vegetation index	Estimated from MOD09Q1 reflectance	250 m	Daily	Whole growing season	
ρ	Dry matter partitioning coefficient	Destructive dry mass (CRK)	*in-situ*	Daily	DOY 204, 209, 215, 224, 238, and 252 in 2015; DOY 125, 132, 138, 146, 151, 159, 169, 180, 190, 201, 214, 224, 232, and 245 in 2016 (there was no data for roots on 125, 132, 190, 214, and 232 in 2016)	BESS-Rice development and input parameters
W	Dry mass of whole rice plant at harvest time (g m^{-2})	Destructive dry mass (CRK2016)	*in-situ*	Daily	at harvest time	
C_m	Grain moisture content at harvest time	Destructive measurement (CRK2016, CFK)	*in-situ*	Daily	at harvest time	
GPP	Gross primary productivity (mg CO_2 m^{-2} s^{-1})	CSAT3 & Li-7200 (CRK, CFK); CSAT3 & Li-7500 (GRK)	*in-situ*	Daily	Whole growing season	BESS-Rice evaluation
Yield	Grain yield (kg ha^{-1})	Destructive yield (all sites)	*in-situ*	Annual	at harvest time	

References

Ainsworth, E.A., 2008. Rice production in a changing climate: a meta-analysis of responses to elevated carbon dioxide and elevated ozone concentration. Glob. Change Biol. 14 (7), 1642–1650.

Asseng, S., Zhu, Y., Wang, E., Zhang, W., 2015. Crop modeling for climate change impact and adaptation. In: Sadras, V.O., Calderini, D.F. (Eds.), Crop Physiology. Academic Press, San Diego, CA, USA pp. 505–546.

Badgley, G., Field, C.B., Berry, J.A., 2017. Canopy near-infrared reflectance and terrestrial photosynthesis. Sci. Adv. 3 (3), e1602244. http://dx.doi.org/10.1126/sciadv.1602244.

Ball, J.T., 1988. An Analysis of Stomatal Conductance. Stanford University, Stanford.

Battude, M., et al., 2016. Estimating maize biomass and yield over large areas using high spatial and temporal resolution sentinel-2 like remote sensing data. Remote Sens. Environ. 184, 668–681.

Belder, P., Bouman, B.A.M., Spiertz, J.H.J., 2007. Exploring options for water savings in lowland rice using a modelling approach. Agric. Syst. 92 (1–3), 91–114.

Best, M.J., et al., 2011. The Joint UK Land Environment Simulator (JULES), model description – part 1: energy and water fluxes. Geosci. Model. Dev. 4 (3), 677–699.

Boote, K.J., Jones, J.W., White, J.W., Asseng, S., Lizaso, J.I., 2013. Putting mechanisms into crop production models. Plant Cell Environ. 36 (9), 1658–1672.

Bouman, B.A.M., et al., 2001. ORYZA2000: Modeling Lowland Rice. International Rice Research Institute.

Bregaglio, S., et al., 2017. Identifying trends and associated uncertainties in potential rice production under climate change in Mediterranean areas. Agric. For. Meteorol. 237, 219–232.

Burke, M., Lobell, D.B., 2017. Satellite-based assessment of yield variation and its determinants in smallholder African systems. Proc. Nat. Acad. Sci. U. S. A 114 (9), 2189–2194.

Cao, W., Moss, D., 1997. Modelling phasic development in wheat: a conceptual integration of physiological components. J. Agric. Sci. 129 (2), 163–172.

Casa, R., et al., 2012. Forcing a wheat crop model with LAI data to access agronomic variables: evaluation of the impact of model and LAI uncertainties and comparison with an empirical approach. Eur. J. Agron. 37 (1), 1–10.

Clark, D.B., et al., 2011. The Joint UK Land Environment Simulator (JULES), model description – part 2: carbon fluxes and vegetation dynamics. Geosci. Model. Dev. 4 (3), 701–722.

De Pury, D., Farquhar, G., 1997. Simple scaling of photosynthesis from leaves to canopies without the errors of big-leaf models. Plant Cell Environ. 20 (5), 537–557.

Dente, L., Satalino, G., Mattia, F., Rinaldi, M., 2008. Assimilation of leaf area index derived from ASAR and MERIS data into CERES-wheat model to map wheat yield. Remote Sens. Environ. 112 (4), 1395–1407.

Dorigo, W.A., et al., 2007. A review on reflective remote sensing and data assimilation techniques for enhanced agroecosystem modeling. Int. J. Appl. Earth Obs. Geoinf. 9 (2), 165–193.

Eklundh, L., Jönsson, P., 2016. TIMESAT for processing time-series data from satellite sensors for land surface monitoring. In: Jarocińska, A., van der Meer, F.D. (Eds.), Multitemporal Remote Sensing. Springer, pp. 177–194.

Fang, H., Wei, S., Liang, S., 2012. Validation of MODIS and CYCLOPES LAI products using global field measurement data. Remote Sens. Environ. 119, 43–54.

Farquhar, G.D., von Caemmerer, S., Berry, J.A., 1980. A biochemical model of photosynthetic CO_2 assimilation in leaves of C3 species. Planta 147, 78–90.

Fick, S.E., Hijmans, R.J., 2017. WorldClim 2: new 1-km spatial resolution climate surfaces for global land areas. Int. J. Climatol. 37 (12), 4302–4315.

Folberth, C., et al., 2016a. Uncertainties in global crop model frameworks: effects of cultivar distribution, crop management and soil handling on crop yield estimates. Biogeosci. Disc. 1–30.

Folberth, C., et al., 2016b. Uncertainty in soil data can outweigh climate impact signals in global crop yield simulations. Nat. Commun. 7. http://dx.doi.org/10.1038/ncomms11872.

Fumoto, T., Kobayashi, K., Li, C., Yagi, K., Hasegawa, T., 2008. Revising a process-based biogeochemistry model (DNDC) to simulate methane emission from rice paddy fields under various residue management and fertilizer regimes. Glob. Change Biol. 14 (2), 382–402.

Fumoto, T., Yanagihara, T., Saito, T., Yagi, K., 2010. Assessment of the methane mitigation potentials of alternative water regimes in rice fields using a process-based biogeochemistry model. Glob. Change Biol. 16 (6), 1847–1859.

Gaydon, D., et al., 2012a. Rice in cropping systems—modelling transitions between flooded and non-flooded soil environments. Eur. J. Agron. 39, 9–24.

Gaydon, D., Probert, M., Buresh, R., Meinke, H., Timsina, J., 2012b. Modelling the role of algae in rice crop nutrition and soil organic carbon maintenance. Eur. J. Agron. 39, 35–43.

Gifford, R.M., 1995. Whole plant respiration and photosynthesis of wheat under increased CO_2 concentration and temperature: long-term vs. short-term distinctions for modelling. Glob. Change Biol. 1 (6), 385–396.

Gitelson, A.A., et al., 2006. Relationship between gross primary production and chlorophyll content in crops: implications for the synoptic monitoring of vegetation productivity. J. Geophys. Res. 111, D08S.

Goudriaan, J., 1977. Crop micrometeorology: A simulation study. Doctoral Dissertation. Pudoc.

Guan, K., et al., 2016. Improving the monitoring of crop productivity using spaceborne solar-induced fluorescence. Glob. Change Biol. 22 (2), 716–726.

Hochman, Z., et al., 2009. Re-inventing model-based decision support with Australian dryland farmers. 4. Yield Prophet® helps farmers monitor and manage crops in a variable climate. Crop Past. Sci. 60 (11), 1057–1070.

Hodson, D., White, J., 2010. GIS and crop simulation modelling applications in climate change research. In: Reynolds, M.P. (Ed.), Climate Change and Crop Production. CABI, Cambridge, MA pp. 245–262.

Hong, J.-K., et al., 2009a. Standardization of KoFlux eddy-covariance data processing. Korean J. Agric. For. Meteorol. 11 (1), 19–26.

Hong, S.Y., et al., 2009b. An introduction of Korean soil information system. Korean J. Soil Sci. Fert. 42 (1), 21–28.

Huang, Y., Zhang, W., Sun, W., Zheng, X., 2007. Net primary production of Chinese croplands from 1950 to 1999. Ecol. Appl. 17 (3), 692–701.

Huang, Y., Zhu, Y., Li, W., Cao, W., Tian, Y., 2013. Assimilating remotely sensed information with the wheatgrow model based on the ensemble square root filter for improving regional wheat yield forecasts. Plant Prod. Sci. 16 (4), 352–364.

Jiang, C., Ryu, Y., 2016. Multi-scale evaluation of global gross primary productivity and evapotranspiration products derived from Breathing Earth System Simulator (BESS). Remote Sens. Environ. 186, 528–547.

Jiang, C., et al., 2017. Inconsistencies of interannual variability and trends in long-term satellite leaf area index products. Glob. Change Biol. 23 (10), 4133–4146.

Jin, X., et al., 2017. Winter wheat yield estimation based on multi-source medium resolution optical and radar imaging data and the aquaCrop model using the particle swarm optimization algorithm. Int. J. Photogramm. Remote Sens. 126, 24–37.

Kang, M., Kim, J., Malla Thakuri, B., Chun, J., Cho, C., 2017. New techniques for gap-filling and partitioning of H_2O and CO_2 eddy fluxes measured over forests in complex mountainous terrain. Biogeosci. Disc. 1–36.

Kassie, B.T., Asseng, S., Porter, C.H., Royce, F.S., 2016. Performance of DSSAT-Nwheat across a wide range of current and future growing conditions. Eur. J. Agron. 81, 27–36.

Kim, H.Y., Ko, J., Kang, S., Tenhunen, J., 2013. Impacts of climate change on paddy rice yield in a temperate climate. Glob. Change Biol. 19 (2), 548–562.

Kim, J., et al., 2011. Relationship between grain filling duration and leaf senescence of temperate rice under high temperature. Field Crops Res. 122 (3), 207–213.

Kim, Y., et al., 2016. Interannual variations in methane emission from an irrigated rice paddy caused by rainfalls during the aeration period. Agric. Ecosyst. Environ. 223, 67–75.

Kobayashi, H., Iwabuchi, H., 2008. A coupled 1-D atmosphere and 3-D canopy radiative transfer model for canopy reflectance, light environment, and photosynthesis simulation in a heterogeneous landscape. Remote Sens. Environ. 112 (1), 173–185.

Li, T., et al., 2015. Uncertainties in predicting rice yield by current crop models under a wide range of climatic conditions. Glob. Change Biol. 21 (3), 1328–1341.

Li, T., et al., 2013. Simulation of genotype performances across a larger number of environments for rice breeding using ORYZA2000. Field Crops Res. 149, 312–321.

Lloyd, J., Taylor, J., 1994. On the temperature dependence of soil respiration. Funct. Ecol. 8, 315–323.

Lobell, D., et al., 2002. Satellite estimates of productivity and light use efficiency in United States agriculture, 1982–98. Glob. Change Biol. 8 (8), 722–735.

Lobell, D.B., Thau, D., Seifert, C., Engle, E., Little, B., 2015. A scalable satellite-based crop yield mapper. Remote Sens. Environ. 164, 324–333.

Maclean, J., Hardy, B., Hettel, G., 2013. Rice Almanac: Source Book for One of the Most Important Economic Activities on Earth. IRRI.

Marino, S., Hogue, I.B., Ray, C.J., Kirschner, D.E., 2008. A methodology for performing global uncertainty and sensitivity analysis in systems biology. J. Theor. Biol. 254 (1), 178–196.

Masutomi, Y., Ono, K., Mano, M., Maruyama, A., Miyata, A., 2016a. A land surface model combined with a crop growth model for paddy rice (MATCRO-rice v. 1)-part 1: model description. Geosci. Model. Dev. 9 (11), 4133–4154.

Masutomi, Y., et al., 2016b. A land surface model combined with a crop growth model for paddy rice (MATCRO-rice v. 1)–Part 2: model validation. Geosci. Model. Dev. 9 (11), 4155–4167.

Messina, C., Hammer, G., Dong, Z., Podlich, D., Cooper, M., 2009. Modelling crop improvement in a G × E × M framework via gene–trait–phenotype relationships. In: Sadras, V., Calderini, D.F. (Eds.), Crop Physiology: Applications for Genetic Improvement and Agronomy. Academic Press, San Diego, CA, USA pp. 235–265.

Min, S.-H., et al., 2013. Seasonal variation of carbon dioxide and energy fluxes during the rice cropping season at rice-barley double cropping paddy field of Gimje. Korean J. Agric. For. Meteorol. 15 (4), 273–281.

Monteith, J.L., 1965. Evaporation and environment. Symp. Soc. Exp. Biol. 205–234.

Mousivand, A., Menenti, M., Gorte, B., Verhoef, W., 2014. Global sensitivity analysis of the spectral radiance of a soil–vegetation system. Remote Sens. Environ. 145, 131–144.

Okawa, S., Makino, A., Mae, T., 2003. Effect of irradiance on the partitioning of assimilated carbon during the early phase of grain filling in rice. Ann. Bot. 92 (3), 357–364.

Paw U, K.T., 1987. Mathematical analysis of the operative temperature and energy budget. J. Therm. Biol. 12 (3), 227–233.

Paw U, K.T., Gao, W., 1988. Applications of solutions to non-linear energy budget equations. Agric. For. Meteorol. 43 (2), 121–145.

Peel, M.C., Finlayson, B.L., McMahon, T.A., 2007. Updated world map of the Koppen-Geiger climate classification. Hydrol. Earth Syst. Sci. 11 (5), 1633–1644.

Peng, Y., Gitelson, A.A., Sakamoto, T., 2013. Remote estimation of gross primary productivity in crops using MODIS 250&xa0;m data. Remote Sens. Environ. 128 (0), 186–196.

Penning de Vries, F.W.T., Jansen, D.M., ten Berge, H.F.M., Bakema, A., 1989. Simulation of ecophysiological processes of growth of several annual crops. Simulation Monographs. Centre for Agricultural Publishing and Documentation (Pudoc)., Wageningen, Netherlands, pp. 82–88.

Priesack, E., Gayler, S., 2009. Agricultural crop models: concepts of resource acquisition and assimilate partitioning. In: Lüttge, U., Beyschlag, W., Büdel, B., Francis, D. (Eds.),

Progress in Botany. Springer, Berlin, Germany pp. 195–222.
Ramirez-Villegas, J., Koehler, A.-K., Challinor, A.J., 2017. Assessing uncertainty and complexity in regional-scale crop model simulations. Eur. J. Agron. 88, 84–95.
Reddy, P.P., 2016. Sustainable Intensification of Crop Production. Springer, Netherlands.
Reichstein, M., et al., 2005. On the separation of net ecosystem exchange into assimilation and ecosystem respiration: review and improved algorithm. Glob. Change Biol. 11 (9), 1424–1439.
Rienecker, M.M., et al., 2011. MERRA: NASA's modern-era retrospective analysis for research and applications. J. Clim. 24 (14), 3624–3648.
Ritchie, J., Singh, U., Godwin, D., Bowen, W., 1998. Cereal growth, development and yield. In: Tsuji, G.Y., Hoogenboom, G., Thornton, P.K. (Eds.), Understanding Options for Agricultural Production. Springer, Netherlands pp. 79–98.
Rosenzweig, C., et al., 2014. Assessing agricultural risks of climate change in the 21st century in a global gridded crop model intercomparison. Proc. Nat. Acad. Sci. U. S. A 111 (9), 3268–3273.
Ryu, Y., et al., 2012. On the temporal upscaling of evapotranspiration from instantaneous remote sensing measurements to 8-day mean daily-sums. Agric. For. Meteorol. 152, 212–222.
Ryu, Y., et al., 2011. Integration of MODIS land and atmosphere products with a coupled-process model to estimate gross primary productivity and evapotranspiration from 1 km to global scales. Glob. Biogeochem. Cycles 25 (GB4017). http://dx.doi.org/10.1029/2011GB004053.
Ryu, Y., Jiang, C., Kobayashi, H., Detto, M., 2018. MODIS-derived global land products of shortwave radiation and diffuse and total photosynthetically active radiation at 5 km resolution from 2000. Remote Sens. Environ. 204, 812–825.
Salomon, J.G., Schaaf, C.B., Strahler, A.H., Gao, F., Jin, Y., 2006. Validation of the MODIS bidirectional reflectance distribution function and albedo retrievals using combined observations from the aqua and terra platforms. IEEE Trans. Geosci. Remote Sens. 44 (6), 1555–1565.
Saltelli, A., et al., 2008. Global Sensitivity Analysis: The Primer. John Wiley & Sons, Ltd.
Saltelli, A., Tarantola, S., Chan, K.-S., 1999. A quantitative model-independent method for global sensitivity analysis of model output. Technometrics 41 (1), 39–56.
Setiyono, T., et al., 2018. Spatial rice yield estimation based on MODIS and Sentinel-1 SAR data and ORYZA crop growth model. Remote Sens. 10 (2), 293.
Sharkey, T.D., Bernacchi, C.J., Farquhar, G.D., Singsaas, E.L., 2007. Fitting photosynthetic carbon dioxide response curves for C(3) leaves. Plant Cell Environ. 30 (9), 1035–1040.
Simelton, E., et al., 2012. The socioeconomics of food crop production and climate change vulnerability: a global scale quantitative analysis of how grain crops are sensitive to drought. Food Secur. 4 (2), 163–179.
Sims, D.A., Gamon, J.A., 2002. Relationships between leaf pigment content and spectral reflectance across a wide range of species, leaf structures and developmental stages. Remote Sens. Environ. 81 (2–3), 337–354.
Singh, U., Ritchie, J.T., Godwin, D., 1993. A User's Guide to CERES Rice, V2. 10. International Fertilizer Development Center, Muscle Shoals, AL, USA.
Sus, O., et al., 2010. A linked carbon cycle and crop developmental model: description and evaluation against measurements of carbon fluxes and carbon stocks at several European agricultural sites. Agric. Ecosyst. Environ. 139 (3), 402–418.
Tang, L., et al., 2009. RiceGrow: A rice growth and productivity model. NJAS-Wageningen J. Life Sci. 57 (1), 83–92.
Tao, F., et al., 2018. Contribution of crop model structure, parameters and climate projections to uncertainty in climate change impact assessments. Glob. Change Biol. 24 (3), 1291–1307.
Thenkabail, P.S., Smith, R.B., De Pauw, E., 2000. Hyperspectral vegetation indices and their relationships with agricultural crop characteristics. Remote Sens. Environ. 71 (2), 158–182.
Tilman, D., Balzer, C., Hill, J., Befort, B.L., 2011. Global food demand and the sustainable intensification of agriculture. Proc. Nat. Acad. Sci. U. S. A 108 (50), 20260–20264.
Timsina, J., Humphreys, E., 2006. Performance of CERES-rice and CERES-wheat models in rice–wheat systems: a review. Agric. Syst. 90 (1-3), 5–31.
Tollenaar, M., Fridgen, J., Tyagi, P., Stackhouse Jr, P.W., Kumudini, S., 2017. The contribution of solar brightening to the US maize yield trend. Nat. Clim. Change 7 (4), 275–278.
Van den Hoof, C., Hanert, E., Vidale, P.L., 2011. Simulating dynamic crop growth with an adapted land surface model – JULES-SUCROS: Model development and validation. Agric. For. Meteorol. 151 (2), 137–153.
Vanuytrecht, E., Raes, D., Willems, P., 2014. Global sensitivity analysis of yield output from the water productivity model. Environ. Model. Softw. 51, 323–332.
Varella, H., Buis, S., Launay, M., Guérif, M., 2012. Global sensitivity analysis for choosing the main soil parameters of a crop model to be determined. Agric. Sci. 3 (7), 949–961.
Verrelst, J., et al., 2015. Global sensitivity analysis of the SCOPE model: what drives simulated canopy-leaving sun-induced fluorescence? Remote Sens. Environ. 166, 8–21.
Wang, Y.P., Leuning, R., 1998. A two-leaf model for canopy conductance, photosynthesis and partitioning of available energy I: model description and comparison with a multi-layered model. Agric. For. Meteorol. 91 (1), 89–111.
Wei, S., Fang, H., 2016. Estimation of canopy clumping index from MISR and MODIS sensors using the normalized difference hotspot and darkspot (NDHD) method: the influence of BRDF models and solar zenith angle. Remote Sens. Environ. 187, 476–491.
Wheeler, T., Von Braun, J., 2013. Climate change impacts on global food security. Science 341 (6145), 508–513.
Wu, X., et al., 2016. ORCHIDEE-CROP (v0), a new process-based agro-land surface model: model description and evaluation over Europe. Geosci. Model. Dev. 9 (2), 857–873.
Xia, J., Yuan, W., Wang, Y.P., Zhang, Q., 2017. Adaptive carbon allocation by plants enhances the terrestrial carbon sink. Sci. Rep. 7 (1), 3341.
Xiao, Y., Zhao, W., Zhou, D., Gong, H., 2014. Sensitivity analysis of vegetation reflectance to biochemical and biophysical variables at leaf, canopy, and regional scales. IEEE Trans. Geosci. Remote Sens. 52 (7), 4014–4024.
Xie, Y., et al., 2017. Assimilation of the leaf area index and vegetation temperature condition index for winter wheat yield estimation using landsat imagery and the CERES-wheat model. Agric. For. Meteorol. 246, 194–206.
Xin, F., et al., 2017. Modeling gross primary production of paddy rice cropland through analyses of data from CO_2 eddy flux tower sites and MODIS images. Remote Sens. Environ. 190, 42–55.
Xin, Q., et al., 2013. A production efficiency model-based method for satellite estimates of corn and soybean yields in the midwestern US. Remote Sens. 5 (11), 5926–5943.
Yang, P., et al., 2007. Evaluation of MODIS land cover and LAI products in cropland of North China plain using in situ measurements and landsat TM images. IEEE Trans. Geosci. Remote Sens. 45 (10), 3087–3097.
Yuan, W., et al., 2016. Estimating crop yield using a satellite-based light use efficiency model. Ecol. Indic. 60, 702–709.
Zhang, L., et al., 2016. Estimating wheat yield by integrating the WheatGrow and PROSAIL models. Field Crops Res. 192, 55–66.
Zhao, G., et al., 2015. Effect of weather data aggregation on regional crop simulation for different crops, production conditions, and response variables. Clim. Res. 65, 141–157.
Zhou, S., et al., 2016. Explaining inter-annual variability of gross primary productivity from plant phenology and physiology. Agric. For. Meteorol. 226–227, 246–256.